Molecular simulations of the *n*-alkane liquid-vapor interface: Interfacial properties and their long range corrections

C. Ibergay,[1] A. Ghoufi,[1] F. Goujon,[1] P. Ungerer,[2] A. Boutin,[3]
B. Rousseau,[3] and P. Malfreyt[1,*]
[1]*Laboratoire de Thermodynamique des Solutions et des Polymères, UMR 6003 CNRS, Université Blaise Pascal, 63177 Aubière Cedex, France*
[2]*Institut Français du Pétrole, 1-4 av. de Bois Préau, 92852 Rueil Malmaison, France*
[3]*Laboratoire de Chimie Physique, UMR 8000 CNRS, Université Paris-Sud, 91405 Orsay Cedex, France*
(Received 12 September 2006; revised manuscript received 6 March 2007; published 3 May 2007)

Monte Carlo simulations have been performed to study the interfacial properties of the liquid-vapor interface of alkanes. We highlight the chemical equilibrium of the liquid-vapor interface by calculating a local chemical potential including the appropriate long-range corrections profiles. We extend the "test-area" (TA) technique developed by Gloor *et al.* [J. Chem. Phys. **123**, 134703 (2005)] on Lennard-Jones and square-well fluids to molecular systems. We establish both operational expressions of the TA approach for the calculation of the surface tension profile and the corresponding long-range corrections by underlining the approximations used. We compare the results between the different operational expressions of the surface tension and focus on the truncation procedures to explain the difference between the different techniques using either the potential or force equations. We make the results of surface tension identical between the different methods by using consistent potential and force equations. In the case of a relatively small cutoff, we propose to show that the Irving-Kirkwood definition and TA methods lead to the same value of the surface tension under condition that appropriate long-range corrections be included in the calculation. We end this paper by calculation of the entropy change profile and a comparison with experiments.

DOI: 10.1103/PhysRevE.75.051602 PACS number(s): 68.03.−g

I. INTRODUCTION

The major advantages of the direct molecular simulation of two-phase systems concern the calculation of the surface tension and a microscopic description of the interfacial region. The difficulties of this method are directly related to the nature of the system—i.e., the nonuniformity of the local density along the direction normal to the surface. This heterogeneity makes problems concerning the truncation procedures involved in the calculation of the potential and corresponding force, the long-range corrections to apply to the macroscopic properties, and the simulation time required to stabilize the interface.

As concerns the truncation procedures, some recent papers [1,2] have shown the importance of the truncation of the potential at the cutoff radius on the mechanical equilibrium and interfacial properties. The fact that the potential is not differentiable at the cutoff value makes the use of the corresponding force not consistent and explains the diversity of the results obtained in Lennard-Jones (LJ) fluids with Monte Carlo (MC) and molecular dynamics (MD) methods. Trokhymchuk and Alejandre [1] have shown that the two methods, MC and MD, are consistent under condition that an impulsive contribution be added to the force to counteract the discontinuous change of the truncated potential at the cutoff distance. The introduction of this additional force does not resolve the difficulties of applying the long-range corrections to the thermodynamic properties in heterogeneous systems. To avoid both the use of these long-range contributions and the discontinuities in the potential and force equations, we have recently performed MC and MD simulations with consistent potential and force by taking the force and its derivative zero at the cutoff value. Using such a modified potential and force, we have shown that the MC and MD methods yield similar coexistence and interfacial properties [2].

Whereas the most commonly used methods [3–7] for the surface tension calculation are based upon the mechanical route definition and use the derivative of the potential in their operational expressions, a novel method called the "test-area" (TA) method [8] based on the thermodynamic definition of the surface tension makes only use of the configurational energy. We propose to show that the surface tension calculated from the gradient of potential (virial route) matches very well with that resulting from the configurational energy (test-area method) when the discontinuities in the potential and force equations are removed. The test-area method uses the perturbation formalism and takes advantage of expressing the surface tension as a difference of energy between a reference state and a perturbed state characterized by an infinitesimal increase or decrease of the surface.

As the most common force fields have been established from simulations using either a truncated potential or a truncated force, the simulations using a potential modified by a switching function are used only as an aid to check the influence of the discontinuities and cannot be used without readjustment to yield quantitative thermodynamic properties in line with the corresponding experimental ones. The long-range corrections become then essential to account for the long-range interactions in the case of the use of truncated potentials. These tail corrections are avoided in most of mo-

*Electronic address: Patrice.MALFREYT@univ-bpclermont.fr

lecular simulations of heterogeneous systems by applying a cutoff radius larger than that used in standard homogeneous molecular simulations. It was observed [1] that the surface tension becomes independent of the cutoff when it is close or larger than 5.5σ. This value corresponds to an effective cutoff radius of 20.5 Å in the case of methane. Our objective was to use a relatively small cutoff to make the two-phase simulation competitive at the level of CPU time with the Gibbs ensemble Monte Carlo (GEMC) method [9–11]. In this case, the use of the long-range corrections to be added to the interfacial properties is meaningful. We have also shown [12] that the value of the surface tension calculated from MC simulations becomes independent of that of the cutoff radius once the long-range corrections are included.

In the case of a planar liquid-vapor surface lying in the x,y plane, the heterogeneity takes place in the z axis normal to the interface. When a two-phase simulation is performed, it is essential to check that some local thermodynamic properties (temperature, pressure, chemical potential) are constant as required for a system at the thermodynamic equilibrium. Some local functions such as the components of the pressure tensor and intermolecular energy contribution cannot be defined unambiguously and must satisfy some constraints. We propose to give the operational expressions of the local temperature, chemical potential, and normal and tangential pressure components by recalling the approximations used to build them.

It is also of basic interest for a test of equilibrium to show that the local total chemical potential is constant throughout the system as it is inhomogeneous in density. Only a few studies have reported the calculation of the chemical potential in very heterogenous systems [13–18]. It is also fundamental to show how the chemical potential is required to be corrected by long-range contributions to keep the same value at the interface and in the bulk phases. We thus implement the modified test-particle [13] insertion method introduced by Widom [19] for homogenous systems in the case of the liquid-vapor surface of methane and discuss the importance of the long-range corrections (LRCs) established by Guo and Lu [20] on the profile of the chemical potential. We also propose to extend the insertion method used for the calculation of the local chemical potential to the calculation of a local entropy contribution.

The calculation of the surface tension will be carried out using different approaches involving either the potential energy or its derivative. When the potential used is truncated, we propose to establish that the different calculations of the surface tension are equivalent under condition that appropriate long-range corrections are added. Within the test-area technique, we propose then to establish the operational expressions of the local surface tension and of the corresponding local long-range corrections by underlining the different approximations used.

The paper is organized as follows. Section II contains the description of the intramolecular and intermolecular potentials and simulation techniques used in this work. Section III contains the different expressions for the calculation of the chemical potential, temperature, and pressure components profiles. Section IV presents the test-area method and the extension of this technique for the calculation of the surface tension and its long-range corrections profiles. Section V presents the different results with appropriate discussions and Sec. VI our conclusions.

II. SIMULATION METHODOLOGY

A. Potential model

The *n*-alkanes are modeled using the united-atom TraPPE [21] description. The sites a and b on different molecules ($i \neq j$) and sites on the same molecule ($i=j$), separated by more than three bonds, interact through a Lennard-Jones potential

$$\mathcal{U}_{\mathrm{LJ}}(r_{iajb}) = 4\epsilon_{ab}\left[\left(\frac{\sigma_{ab}}{r_{iajb}}\right)^{12} - \left(\frac{\sigma_{ab}}{r_{iajb}}\right)^{6}\right], \tag{1}$$

where r_{iajb} is the distance between atom a in molecule i and atom b in molecule j, ϵ_{ab} is the energy parameter of the interaction, and σ_{ab} is the Lennard-Jones core diameter. The LJ parameters for the interactions between sites a and b are calculated by using the Lorentz-Berthelot mixing rules:

$$\epsilon_{ab} = (\epsilon_{aa}\epsilon_{bb})^{1/2}, \quad \sigma_{ab} = \frac{1}{2}(\sigma_{aa} + \sigma_{bb}). \tag{2}$$

The interaction sites have the following Lennard-Jones parameters: $\epsilon_{\mathrm{CH_4}}/k_B = 148$ K, $\epsilon_{\mathrm{CH_3}}/k_B = 98$ K, and $\epsilon_{\mathrm{CH_2}}/k_B = 46$ K where k_B is Boltzmann's constant. The size parameters are $\sigma_{\mathrm{CH_4}} = 3.73$ Å, $\sigma_{\mathrm{CH_3}} = 3.75$ Å, and $\sigma_{\mathrm{CH_2}} = 3.95$ Å.

The bond distance between two sites is fixed at the separation of 1.54 Å. The bond-angle interactions are harmonic, with

$$u_{\mathrm{bend}} = \frac{1}{2}k_\theta(\theta - \theta_0)^2, \tag{3}$$

where θ is the angle between three consecutive united atoms, $k_\theta/k_B = 62\,500$ K rad^{-2} is the bending constant, and $\theta_0 = 114°$ is the equilibrium bond angle.

In the case of the modeling of the *n*-pentane and *n*-decane molecules, the torsional potentials are represented by the OPLS potential model [22]

$$u_{tors} = c_1(1 + \cos\phi) + c_2(1 - \cos 2\phi) + c_3(1 + \cos 3\phi), \tag{4}$$

where ϕ is the dihedral angle between four subsequent united atoms, $c_1/k_B = 355.03$ K, $c_2/k_B = -68.19$ K, and $c_3/k_B = 791.32$ K.

B. Computational procedures

The simulation box is a rectangular parallelepipedic box of dimensions $L_xL_yL_z(L_x=L_y)$ with N alkane molecules. The details of the geometry of the system and the total number of molecules are given in Table I. The periodic boundary conditions are applied in the three directions. MC simulations are performed in the *NVT* ensemble. Each cycle consists of N randomly selected moves with fixed probabilities. The moves are (i) displacement of the center of mass of a random molecule, (ii) rotation of a randomly selected molecule around

TABLE I. Dimensions of the simulation box, number of alkanes molecules, and relative probabilities for the different types of MC moves.

	methane	*n*-pentane	*n*-decane
$L_x=L_y$ (Å)	40	35	35
L_z (Å)	272	235	400
N	3000	500	300
% (translation)	100	45	35
% (rotation)	0	35	25
% (internal)	0	20	40

its center of mass, and (iii) regrowth of part of a random molecule using the configurational-bias scheme [23]. The relative probabilities for the different types of moves are given in Table I as a function of the alkane chain length. The maximum displacement and maximum rotation are adjusted during the equilibration phase to give an acceptance ratio of 0.4. As concerns the translational moves, two different displacements have been chosen randomly with equal probability. The adjustment of these two maximum displacements, during the equilibration phase, gives acceptance ratios of 20% and 60%. This specificity for the translational moves improves the sampling of the configurational space of the vapor phase.

The initial configuration has been built by placing N alkane molecules on a cubic box with random positions. MC simulations in the NpT ensemble have been performed on this bulk fluid configuration. The dimension of the resulting box has been increased along the z axis by placing two empty cells on both sides of the bulk liquid box. A typical MC run consists of 100 000 cycles for equilibration and 200 000 cycles for the production phase. The configurational temperature, the normal and tangential components of the pressure tensor, the surface tension, and the chemical potential are calculated every 10 cycles. The statistical errors in these properties are estimated using 10 blocks averages of 2000 configurations. As the geometry of the system shows an heterogeneity along the axis normal to the interface (z axis), we expect thus a dependence of the thermodynamic properties only in this direction. We have therefore calculated the temperature, pressure, and surface tension and its long-range correction as a function of z_k by splitting the cell into slabs of width δz.

III. THERMODYNAMIC EQUILIBRIA

In a classical system constituted by N identical particles of mass m defined by their coordinates $\mathbf{r}^N$ and momenta $\mathbf{p}^N$, the Helmholtz free energy F is related to the partition function Q_{NVT} in the constant-NVT ensemble by the following expression:

$$F = -k_B T \ln Q_{NVT} \tag{5}$$

$$= -k_B T \ln\left[\frac{1}{h^{3N} N!}\int\int d\mathbf{r}^N d\mathbf{p}^N \exp\left(-\frac{\mathcal{H}(\mathbf{r}^N,\mathbf{p}^N)}{k_B T}\right)\right] \tag{6}$$

$$= -k_B T \ln\left[\frac{1}{\Lambda^{3N} N!}\int d\mathbf{r}^N \exp\left(-\frac{\mathcal{U}(\mathbf{r}^N)}{k_B T}\right)\right]. \tag{7}$$

The total Hamiltonian in Eq. (6) can be written as the sum of the kinetic and potential energies of the system. Let us suppose that the potential energy $\mathcal{U}(\mathbf{r}^N)$ is independent of the velocities; the double integral in Eq. (6) can be separated in two integrals, one over the positions and one over the momenta. This latter can be written in terms of the de Broglie thermal wavelength Λ. The resulting expression of the Helmholtz free energy is given by Eq. (7). Let us recall that Eq. (7) is then valid only for rigid or flexible molecules with no internal constraint on bond lengths [24,25].

A. Chemical equilibrium

The chemical potential is the derivative of the Helmholtz free energy with respect to the number of particles, N, and can be expressed for sufficient large N as

$$\begin{aligned}\mu &= -k_B T \frac{\partial \ln Q_{NVT}}{\partial N} = -k_B T \ln \frac{Q_{N+1,VT}}{Q_{NVT}} \\ &= -k_B T \ln \frac{N!\Lambda^{3N}}{(N+1)!\Lambda^{3(N+1)}} \frac{\int d\mathbf{r}^{N+1} \exp\left(-\frac{\mathcal{U}(\mathbf{r}^{N+1})}{k_B T}\right)}{\int d\mathbf{r}^N \exp\left(-\frac{\mathcal{U}(\mathbf{r}^N)}{k_B T}\right)} \\ &= -k_B T \ln \frac{V}{N\Lambda^3} \frac{\int d\mathbf{r}^N \exp(-\Delta\mathcal{U}/k_B T)\exp\left(-\frac{\mathcal{U}(\mathbf{r}^N)}{k_B T}\right)}{\int d\mathbf{r}^N \exp\left(-\frac{\mathcal{U}(\mathbf{r}^N)}{k_B T}\right)}\end{aligned} \tag{8}$$

$$= -k_B T \ln \rho\Lambda^3 - k_B T \ln \langle \exp(-\Delta\mathcal{U}/k_B T)\rangle_{NVT} \tag{9}$$

$$= \mu_{\mathrm{id}} + \mu_{\mathrm{ex}}. \tag{10}$$

The most common method for the calculation of the excess contribution of the chemical potential is the Widom test particle [19] and consists in inserting a ghost particle randomly into a simulation box and calculating the energy of its interaction with the N particles. The operational expression for the calculation of the chemical potential is given in Eq. (9) where $\Delta\mathcal{U}=\mathcal{U}(\mathbf{r}^{N+1})-\mathcal{U}(\mathbf{r}^N)$ represents the energy of interaction of the $(N+1)$th particle with the other N particles. The angular brackets $\langle\cdots\rangle_{NVT}$ denote a canonical ensemble average over the configuration space of the N particles, and ρ is the mean number density expressed in number of particles per m^3. In the case of a system of particles, the first term in Eq. (9) is the ideal gas chemical potential and the second term defines the excess chemical potential of the system. For a system with an inhomogeneity in density in the z direction, the operational expression of μ has been modified by Widom [13] to account for the local dependance of μ on the density ρ. So the full chemical potential $\mu(z)$ depends on the z position, according to Eq. (11):

$$\mu(z_k) = kT \ln\left(\left\langle \frac{\Lambda^3 \rho(z_k)}{\exp(-\Delta\mathcal{U}/k_BT)} \right\rangle_{z_k,NVT}\right)$$

$$\approx kT \ln\left(\frac{\Lambda^3 \langle \rho(z_k)\rangle_{NVT}}{\langle \exp(-\Delta\mathcal{U}/k_BT)\rangle_{z_k,NVT}}\right), \tag{11}$$

where $\rho(z_k)$ is the number density at the position z_k. The right term given in Eq. (11) results from the assumption that the average of the ratio can be replaced by the ratio of the two averages. We check that the difference between $\left\langle \frac{\rho(z_k)}{\exp(-\Delta\mathcal{U}/k_BT)} \right\rangle$ and $\frac{\langle \rho(z_k)\rangle}{\langle \exp(-\Delta\mathcal{U}/k_BT)\rangle}$ is within 10^{-5} unit, indicating that $\langle \rho(z_k)\rangle$ and $\langle \exp(-\Delta\mathcal{U}/k_BT)\rangle$ are uncorrelated. Let us recall that this expression has been established in the mean-field approximation. We recall here some approximations of the mean-field approach. In the case of inhomogeneous fluid within the mean-field approximation, we have to use an additional approximation of a small gradient of density. It means that we have to consider that $\rho(z_k)$ changes slightly over distance comparable with the distance of neighboring particles. On such a scale, the local density $\rho(z_k)$ can be considered as uniform. It follows from this that the local configurational chemical potential in the liquid phase or vapor phase is the same that that calculated for an homogeneous system with a mean density corresponding to that of the local density of the liquid or vapor region. As concerns the interfacial region, the mean approximation considers it as a matter of bulk with a local chemical potential—that is, that of hypothetically uniform fluid with the same density with an additional term taking into account the nonuniformity of this region. The small-gradient approximation becomes accurate when the simulation of the two-phase system is carried out near the critical point. This operational expression of the chemical potential resulting from a certain number of approximations has been already applied in the simulations of the two-phase systems [14–18].

B. Thermal equilibrium

In most computer simulations of equilibrium systems, the temperature was calculated from taking averages of the kinetic energy. From Rugh's result [26], Jepps *et al.* [27] have established a more general expression of Rugh's theorem:

$$k_BT_{\text{conf}} = \frac{\langle \nabla\mathcal{H}(\Gamma)\cdot\mathbf{B}(\Gamma)\rangle}{\langle \nabla\cdot\mathbf{B}(\Gamma)\rangle}, \tag{12}$$

where the angular brackets denote an canonical ensemble average. $\Gamma \equiv (r_1,\ldots,r_{3N},p_1,\ldots,p_{3N})$ is a phase-space vector of an N-particle system where q_i and p_i represent the $6N$ spatial coordinates and conjugate momenta, respectively. The Hamiltonian $\mathcal{H}(\Gamma)$ is equal to the sum of $\mathcal{K}(r_1,\ldots,r_{3N})$ and $\mathcal{U}(r_1,\ldots,r_{3N})$. $\mathbf{B}(\boldsymbol{\Gamma})$ is an arbitrary vector field. If $\mathbf{B}(\boldsymbol{\Gamma}) = (0,\ldots,0,p_1,\ldots,p_{3N})$ depends only upon the momentum of the particles, the temperature is calculated through the equipartition theorem from the kinetic energy. By choosing $\mathbf{B}(\boldsymbol{\Gamma}) = \mathbf{G}\nabla\mathcal{H}$ where the general matrix $\mathbf{G}$ is not unique and by taking the matrix $\mathbf{G}$ such as $g_{ij} = \delta_{ij}$ if i and j refer to coordinate variables and 0 otherwise, $\mathbf{B}(\boldsymbol{\Gamma})$ becomes equal to $\nabla\mathcal{U}$. The expression of the configuration temperature [27,28] becomes to order $1/N$

$$k_BT_{\text{conf}} = \frac{\langle(\nabla\mathcal{U})^2\rangle}{\langle\nabla^2\mathcal{U}\rangle} + O\left(\frac{1}{N}\right). \tag{13}$$

An order-1 operational expression of the configurational expression depending on the first and second spatial derivatives of the intermolecular potential energy is given by

$$k_BT_{\text{conf}} = \frac{\left\langle \sum_{i=1}^{N} \mathbf{F}_i^2 \right\rangle}{\left\langle -\sum_{i=1}^{N}\left(\frac{\partial F_{ix}}{\partial r_{ix}} + \frac{\partial F_{iy}}{\partial r_{iy}} + \frac{\partial F_{iz}}{\partial r_{iz}}\right)\right\rangle}, \tag{14}$$

where r_{ix}, r_{iy}, and r_{iz} refer the Cartesian coordinates of $\mathbf{r}_i$. In the molecular version of the configurational temperature given in Eq. (14), N represents the number of molecules in the system. $\mathbf{F}_i$ is the intermolecular force on molecule i acting upon the molecular center of mass, $\mathbf{r}_i$, and is expressed as

$$\mathbf{F}_i = \sum_{j\neq i}^{N} \mathbf{F}_{ij} = \sum_{j\neq i}^{N}\sum_{a=1}^{N_a}\sum_{b=1}^{N_b} (\mathbf{f}_{iajb}), \tag{15}$$

where N_a and N_b are the number of sites in the molecules i and j, respectively. This is equivalent to expressing $\mathbf{F}_{ij}$ as the sum of all site-site forces acting between molecules. Using this definition, $\mathbf{F}_{ij}$ is then is the intermolecular force between molecules i and j and $\mathbf{f}_{iajb}$ of Eq. (16) is the force between atom a in molecule i and atom b in molecule j:

$$\mathbf{f}_{iajb} = -\frac{\mathbf{r}_{iajb}}{r_{iajb}}\frac{d\mathcal{U}_{\text{LJ}}(r_{iajb})}{dr_{iajb}}. \tag{16}$$

In the case of a system with an inhomogeneity along the z direction, we use a new expression for the matrix $\mathbf{G}$. This definition has been used [29] to calculate the temperature along a specific direction in the case of confined systems. $\mathbf{G}$ is chosen such as $g_{ij} = \delta_{ij}\delta_{ib}\delta_{jb}$ if i and j refer to coordinate variables. δ_{ib} is equal to unity if the atom associated with i is located in the slab k and 0 otherwise. A first-order operational expression of the local configurational expression becomes then

$$k_BT_{\text{conf}}(z_k) = \frac{\left\langle \sum_{i=1,i\in k}^{N} \mathbf{F}_i^2 \right\rangle}{\left\langle -\sum_{i=1,i\in k}^{N}\left(\frac{\partial F_{ix}}{\partial r_{ix}} + \frac{\partial F_{iy}}{\partial r_{iy}} + \frac{\partial F_{iz}}{\partial r_{iz}}\right)\right\rangle}, \tag{17}$$

where i refers to the molecule. This operational expression in Eq. (17) can be used to calculate the temperature in Monte Carlo simulations where the momenta are not known and in heterogeneous systems to check the constancy of this property along a peculiar direction. As the matrix $\mathbf{G}$ is not unique, other operational expressions for the configurational temperature are possible.

C. Mechanical equilibrium

The mechanical stability of a planar liquid-gas surface can be established from the calculation of the normal and tangential components of the pressure tensor as a function of the position along the normal to the surface. The method of Irving and Kirkwood [5] is based upon the notion of the force across a unit area. The pressure tensor is then written as a sum of a kinetic term and a potential term resulting from the intermolecular forces. Whereas the first term is well defined, the potential term is subjected to arbitrariness because there is no unique way to determine which intermolecular forces contribute to the stress across dA. There are many ways of choosing the contour joining two interacting particles. Irving and Kirkwood [5] have chosen as a contour the straight line between the two particles. Other choices [30] are possible and result from the lack of uniqueness in the definition of the microscopic stress tensor. The components of the pressure [3,6,7] tensor in the Irving-Kirkwood definition are expressed as

$$p_{\alpha\beta}(z_k) = \langle \rho(z_k) \rangle k_B T \mathbf{I} - \frac{1}{A} \left\langle \sum_{i=1}^{N-1} \sum_{j>i}^{N} (\mathbf{r}_{ij})_\alpha (\mathbf{F}_{ij})_\beta \frac{1}{|z_{ij}|} \theta\left(\frac{z_k - z_i}{z_{ij}}\right) \theta\left(\frac{z_j - z_k}{z_{ij}}\right) \right\rangle, \tag{18}$$

where $\mathbf{I}$ is the unit tensor and T is the input temperature. α and β represent the x, y, or z direction. $\theta(x)$ is the unit step function defined by $\theta(x)=0$ when $x<0$ and $\theta(x)=1$ when $x \geqslant 0$. A is the surface area normal to the z axis. The distance z_{ij} between two molecular centers of mass is divided into N_s slabs of thickness $\delta z = 1.0$ Å. Following Irving and Kirkwood, the molecules i and j give a local contribution to the pressure tensor in a given slab if the line joining the centers of mass of molecules i and j crosses, starts, or finishes in the slab. Each slab has $1/N_s$ of the total contribution from the i-j interaction. The normal component $p_N(z_k)$ is equal to $p_{zz}(z_k)$ whereas the tangential component is given by $\frac{1}{2}[p_{xx}(z_k) + p_{yy}(z_k)]$. We adopt the molecular definition of the pressure tensor using the center-of-mass definition. This definition is only valid for pairwise additive potentials. Following this definition, the forces arising from the intramolecular interactions (bond-angle distorsions) make no contribution to the molecular pressure tensor.

Todd, Evans, and Daivis [31] have developed a method based upon the continuity equations of hydrodynamics. In previous papers [2,12], we have shown that the local configurational term of the normal component of the pressure tensor calculated from this method matched very well with that resulting from the definition of Irving and Kirkwood in the case of an *n*-pentane liquid-vapor surface.

In the case of a planar surface, the local value of the normal component of the pressure tensor is constant and independent of z_k whereas the tangential part of the pressure tensor is large and negative in the interfacial region and equal to the normal part in the vapor and liquid regions. The calculation of these local components represents a way of checking the mechanical equilibrium of the two-phase systems. This type of calculation for the local components of the pressure tensor has been widely used to establish the mechanical equilibrium of heterogenous systems [1,2,17,32–34].

IV. INTERFACIAL PROPERTIES: SURFACE TENSION CALCULATION

In the constant-NVT ensemble the surface tension γ can be expressed as the derivative of the Helmholtz energy with respect to the interfacial area. In other terms, the surface tension is defined in Eq. (19) as the change in free energy for an infinitesimal change in the area. This infinitesimal change in the area can be performed throughout a perturbed system [state (1)] in which the box dimensions are changed by a small quantity ϵ such as $\epsilon \ll 1$. The box dimensions $(L_x^{(1)}, L_y^{(1)}, L_z^{(1)})$ in the perturbed systems are changed using the transformations $L_x^{(1)} = L_x^{(0)}\sqrt{1+\epsilon}$, $L_y^{(1)} = L_y^{(0)}\sqrt{1+\epsilon}$, and $L_z^{(1)} = L_z^{(0)}/(1+\epsilon)$ where the superscript (0) refers to the reference system [state (0)]. The area $A^{(1)}$ in the perturbed state is changed as $A^{(1)} = L_x^{(0)} L_y^{(0)}(1+\epsilon) = A^{(0)} + \Delta A_\epsilon$ where $\Delta A_\epsilon = L_x^{(0)} L_y^{(0)} \epsilon$. These transformations conserve the volume of the box in the perturbed state. This means that it is possible to express the surface tension as a ratio of partition function between the perturbed and reference states as in Eq. (20). In this equation, $\mathcal{U}^{(0)}(\mathbf{r}^N)$ and $\mathcal{U}^{(1)}(\mathbf{r}'^N)$ are the configurational energies of the systems with an area $A^{(0)}$ and a configurational space $\mathbf{r}^N$ and an area $A^{(1)}$ and a configurational space $\mathbf{r}'^N$, respectively. The transformations used for the change in the volume lead to the equality $d\mathbf{r}'^N = d\mathbf{r}^N$. This expression is the key for writing the surface tension as the average of $\exp\left(-\frac{\Delta \mathcal{U}}{kT}\right)$ in the constant-NVT ensemble [Eqs. (21) and (22)]:

$$\gamma = \left(\frac{\partial F}{\partial A}\right)_{N,V,T} = \lim_{\epsilon \to 0} \frac{F(N,V,T,A^{(1)}) - F(N,V,T,A^{(0)})}{\Delta A_\epsilon} = -\frac{k_B T}{\Delta A_\epsilon} \ln \frac{Q_{NVT}^{(1)}}{Q_{NVT}^{(0)}} \tag{19}$$

$$= -\frac{k_B T}{\Delta A_\epsilon} \ln \frac{\int d\mathbf{r}'^N \exp\left(-\frac{\mathcal{U}^{(1)}(\mathbf{r}'^N)}{k_B T}\right)}{\int d\mathbf{r}^N \exp\left(-\frac{\mathcal{U}^{(0)}(\mathbf{r}^N)}{k_B T}\right)} \tag{20}$$

$$= -\frac{k_B T}{\Delta A_\epsilon} \ln \frac{\int d\mathbf{r}^N \exp\left(-\frac{\mathcal{U}^{(1)}(\mathbf{r}'^N)}{k_B T}\right)}{\int d\mathbf{r}^N \exp\left(-\frac{\mathcal{U}^{(0)}(\mathbf{r}^N)}{k_B T}\right)} \tag{21}$$

$$= -\frac{k_B T}{\Delta A_\epsilon} \times \ln \frac{\int d\mathbf{r}^N \exp\left(-\frac{(\mathcal{U}^{(1)}(\mathbf{r}'^N) - \mathcal{U}^{(0)}(\mathbf{r}^N)}{k_B T}\right) \exp\left(-\frac{\mathcal{U}^{(0)}(\mathbf{r}^N)}{k_B T}\right)}{\int d\mathbf{r}^N \exp\left(-\frac{\mathcal{U}^{(0)}(\mathbf{r}^N)}{k_B T}\right)}. \tag{22}$$

From the perturbation of the interfacial area, we come to the operational expression of the surface tension given in Eq. (23):

$$\gamma_{\mathrm{TA}} = -\frac{k_B T}{2\Delta A_\epsilon} \ln\left\langle \exp\left(-\frac{(\mathcal{U}^{(1)}(\mathbf{r}'^N) - \mathcal{U}^{(0)}(\mathbf{r}^N))}{k_B T}\right)\right\rangle_0 = -\frac{k_B T}{2\Delta A_\epsilon} \ln\left\langle \exp\left(-\frac{\Delta\mathcal{U}}{k_B T}\right)\right\rangle_0, \tag{23}$$

where $\langle\cdots\rangle_0$ denotes the canonical average over the reference system. The factor of $\frac{1}{2}$ is introduced to take into account that the geometry of the system imposes two interfaces. The expression given in Eq. (23) has been recently established by Gloor *et al.* [8] and has led to a novel method called the "test-area" technique. The equivalence between γ_{TA} and the macroscopic definition of the surface tension is given in Appendix A.

In the present paper, we propose a local operational expression of the surface tension based on the test-area method. The derivation of this expression is given with the approximations used in Appendix A. The total surface tension is then approximated by

$$\gamma_{\mathrm{TA}} \approx \frac{1}{2}\sum_{i=1}^{N_s} \gamma_{\mathrm{TA}}(z_k). \tag{24}$$

Writing Eq. (24) amounts to assuming that the energy of the slab at the position z_k is uncorrelated to that of the slab at z_{k+1}. We check this assumption by showing in Fig. 1(a) the $C(z_k)$ function defined by $\left\langle \exp\left(-\frac{\Delta\mathcal{U}_{z_k}}{k_B T}\right)\exp\left(-\frac{\Delta\mathcal{U}_{z_{k+1}}}{k_B T}\right)\right\rangle_{z_k} - \left\langle \exp\left(-\frac{\Delta\mathcal{U}_{z_k}}{k_B T}\right)\right\rangle_{z_k}\left\langle \exp\left(-\frac{\Delta\mathcal{U}_{z_{k+1}}}{k_B T}\right)\right\rangle_{z_{k+1}}$. We observe that this function is within 10^{-6} unit at each z_k, indicating no correlation between the surface tensions of two neighboring slabs. The local surface tension $\gamma(z_k)$ is then given by

$$\gamma_{\mathrm{TA}}(z_k) = -\frac{k_B T}{\Delta A_\epsilon} \ln\left\langle \exp\left(-\frac{\Delta\mathcal{U}_{z_k}}{k_B T}\right)\right\rangle_{z_k}, \tag{25}$$

where $\Delta\mathcal{U}_{z_k}$ represents the difference in the slab potential energy between the reference and perturbed states. A difficulty arises here for the definition of the slab energy. The ambiguity [3] focuses on the part of the interaction energy to be included in the volume V_s of the slab. We adopt the definition of Ladd and Woodcok [35] and choose to assign in the slab centered on z_k two energy contributions: one contribution due to the energy between the molecules within the slab and a second contribution due to the energy of the molecules within the slab with those outside the slab. The energy of the slab at the position z_k is defined as

$$\mathcal{U}_{z_k} = \frac{1}{2}\sum_{i=1}^{N}\sum_{j\neq i}^{N}\sum_{a}^{N_a}\sum_{b}^{N_b} H_k(z_i)\mathcal{U}_{\mathrm{LJ}}(r_{iajb}). \tag{26}$$

Using this definition, we respect the condition

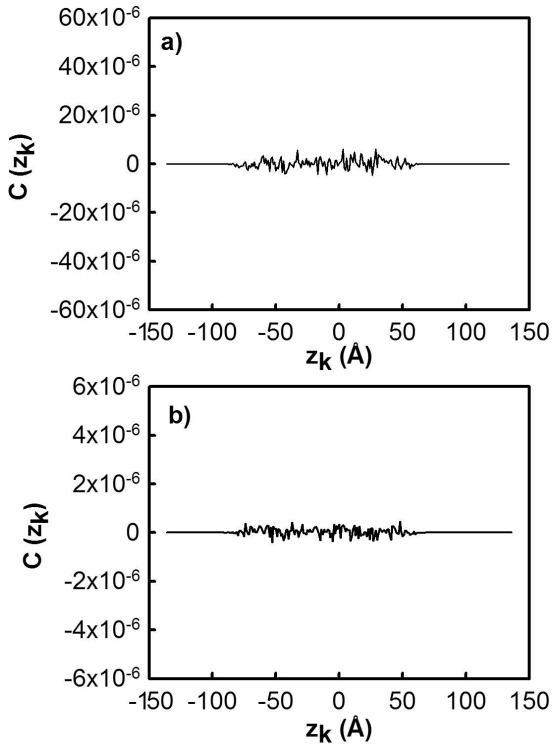

FIG. 1. Calculated local spatial correlation function $C(z_k)$ defined in (a) by $\left\langle \exp\left(-\frac{\Delta\mathcal{U}_{z_k}}{k_B T}\right)\exp\left(-\frac{\Delta\mathcal{U}_{z_{k+1}}}{k_B T}\right)\right\rangle_{z_k} - \left\langle \exp\left(-\frac{\Delta\mathcal{U}_{z_k}}{k_B T}\right)\right\rangle_{z_k}\left\langle \exp\left(-\frac{\Delta\mathcal{U}_{z_{k+1}}}{k_B T}\right)\right\rangle_{z_{k+1}}$ and in (b) by $\left\langle \exp\left(-\frac{(\Delta\mathcal{U}_{z_k}+\Delta\mathcal{U}_{\mathrm{LRC},z_k})}{k_B T}\right)\right\rangle_{z_k} - \left\langle \exp\left(-\frac{(\Delta\mathcal{U}_{z_k})}{k_B T}\right)\right\rangle_{z_k}\left\langle \exp\left(-\frac{(\Delta\mathcal{U}_{\mathrm{LRC},z_k})}{k_B T}\right)\right\rangle_{z_k}$.

$$\int_V dz_k \mathcal{U}_{z_k} = \mathcal{U}_{\mathrm{tot}}, \tag{27}$$

where $\mathcal{U}_{\mathrm{tot}}$ is the total configurational energy of the simulation box and V its volume. As a numerical check of this operational expression, the arithmetical average of the local surface tension over all the slabs must produce the same result as that of Eq. (23).

We note that there is some ambiguity in the definition of the local energy and other definitions are possible. Our aim is to use this local energy contribution as an intermediary for the calculation of the local surface tension from the perturbation formalism. To be satisfactory, the adopted definition must respect the integral given in Eq. (27) and gives a total surface tension in agreement with the different definitions of this property.

From a mechanical viewpoint, the surface tension can be also calculated from the integration of the difference of the normal and tangential components of the pressure tensor of Irving and Kirkwood [3,6,7] across both interfaces according to

$$\gamma_{\mathrm{IK}} = \frac{1}{2}\int_{-L_z/2}^{+L_z/2} dz[p_N(z) - p_T(z)]. \tag{28}$$

This operational expression also provides a profile of the surface tension $\gamma_{IK}(z)$ defined as $[p_N(z) - p_T(z)]\delta z$. The total

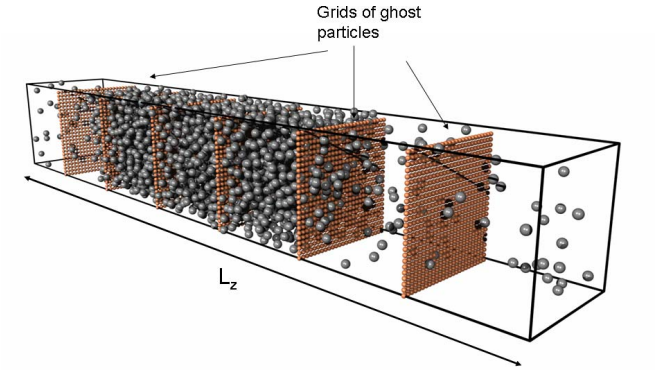

FIG. 2. (Color online) Typical configuration of a methane liquid-vapor interface with grids of ghost particles inserted at different z_k positions. For clarity, we have represented only six grids of ghost particles.

surface tension is then calculated via the half sum of the local surface tension $\gamma_{IK}(z_k)$.

From the local definition of the surface tension, it is possible to obtain an expression by integrating of dz over all space. This expression is referred to as the virial expression of the surface tension and is the same as that resulting from the thermodynamic definition using the derivative of the free energy with respect to the area of the liquid surface. This expression was obtained by Kirkwood and Buff [4] and will be referred as the Buff expression (γ_{Buff}). Some intermediate expressions leading to the final operational expression of Eq. (29) are given for clarity in Appendix A:

$$\gamma_{Buff} = \frac{1}{2A}\left\langle \sum_{i=1}^{N-1}\sum_{j=i+1}^{N}\sum_{a=1}^{N_a}\sum_{b=1}^{N_b} \frac{\mathbf{r}_{ij}\cdot\mathbf{r}_{iajb} - 3z_{ij}z_{iajb}}{2r_{iajb}} \frac{d\mathcal{U}_{LJ}(r_{iajb})}{dr_{iajb}} \right\rangle. \tag{29}$$

V. RESULTS AND DISCUSSIONS

In the first part of this paper, we aim to calculate the different contributions of the chemical potential along the direction normal to the interface. The term $\langle \exp(-\Delta\mathcal{U}/k_BT)\rangle_{z_k}$ is calculated from a grid of ghost particles. Six hundred and twenty-five test particles uniformly distributed in a square plane grid (25×25) are inserted at different z_k positions 1.0 Å apart as shown in Fig. 2. Figure 3(a) shows the profiles of $\mu_{id}(z_k)$ and $\mu_{ex}(z_k)$ calculated from a MC simulation using a truncated LJ potential. Figure 3(b) presents the profiles of the long-range corrections parts where $\mu_{1,LRC}(z_k)$ and $\mu_{2,LRC}(z_k)$ correspond to the first and second terms of the LRC to the chemical potential, established by Guo and Lu [20] and expressed as follows:

$$\begin{aligned}\mu_{LRC}(z_k) &= \mu^{(1)}_{LRC}(z_k) + \mu^{(2)}_{LRC}(z_k)\\ &= 4\pi\rho(z_k)\int_{r_c}^{\infty} dr r^2 \mathcal{U}_{LJ,m}(r) + 2\pi\int_{r_c}^{\infty} dr\\ &\quad\times\int_{-r}^{r} d\Delta z \sum_{i=1}^{N_s}[\rho(z_{k+i}) - \rho(z_{k+i-1})] r\mathcal{U}_{LJ,m}(r),\end{aligned} \tag{30}$$

where $\mathcal{U}_{LJ,m}(r)$ is defined by

$$\mathcal{U}_{LJ,m}(r) = \sum_{a=1}^{N_a}\sum_{b=1}^{N_b} 4\epsilon_{ab}\left[\left(\frac{\sigma_{ab}}{r}\right)^{12} - \left(\frac{\sigma_{ab}}{r}\right)^{6}\right]. \tag{31}$$

Δz is the difference $(z-z_k)$ and varies between $-r$ and r. N_s is the number of slabs between z_k and z. The sum $\Sigma_{i=1}^{N_s}[\rho(z_{k+i}) - \rho(z_{k+i-1})]$ is then equivalent to the difference $\rho(z)-\rho(z_k)$. The first term is similar to that used in homogeneous system except the use of a number of density $\rho(z_k)$ depending on z_k. The second term takes into account that each slab z_k is surrounded with slabs of different local densities.

The profile of $\mu_{id}(z_k)+\mu_{ex}(z_k)$ represented in dotted line in Figs. 3(a) and 2(b) is not uniform across the simulation box with a positive value in the liquid phase. The constancy of the total chemical potential of the methane liquid-vapor surface is reached once two additional long-range correction terms are added. In this case, we show in Fig. 3(b) that the local total chemical potential is constant in the liquid, vapor, and interface regions as expected for a chemical equilibrium. In order to conclusively establish that the long-range corrections of the chemical potential are essential for moderate small cutoffs and truncated potentials, we modify the standard LJ potential by the addition of a polynomial function as in Eq. (32),

$$\mathcal{U}_{SP}(r) = \begin{cases} \mathcal{U}_{LJ}(r) - \mathcal{U}_{LJ}(r_s) + a, & r < r_s,\\ -\dfrac{b}{3}(r-r_c)^3 - \dfrac{c}{4}(r-r_c)^4, & r_s \leqslant r < r_c,\\ 0, & r \geqslant r_c, \end{cases} \tag{32}$$

where the parameters a, b, and c are calculated by requiring that the first and second derivatives of the $\mathcal{U}_{SP}$ potential must be continuous at r_s and r_c:

$$\begin{aligned} c &= -\frac{\dfrac{\partial^2\mathcal{U}_{LJ}}{\partial r^2}(r_s)}{(r_s-r_c)^2} + 2\frac{\dfrac{\partial\mathcal{U}_{LJ}}{\partial r}(r_s)}{(r_s-r_c)^3},\\ b &= \frac{\dfrac{\partial^2\mathcal{U}_{LJ}}{\partial r^2}(r_s)}{(r_s-r_c)} - 3\frac{\dfrac{\partial\mathcal{U}_{LJ}}{\partial r}(r_s)}{(r_s-r_c)^2},\\ a &= -\frac{b}{3}(r_s-r_c)^3 - \frac{c}{4}(r_s-r_c)^4. \end{aligned} \tag{33}$$

We take the cutoff radius $r_c=12$ Å and $r_s=11$ Å. With this expression, no long-range corrections are numerically required because the potential is zero at the cutoff value. Figure 3(c) shows the profiles of $\mu_{id}(z)$ and $\mu_{ex}(z)$ calculated from a MC simulation using a LJ potential modified by a switching function. Figure 3(d) exhibits the profile of $\mu_{id}(z)+\mu_{ex}(z)$ by using the same scale as that used for the profile calculated with a truncated LJ potential. As expected, Fig. 3(d) shows that the total local chemical potential is independent of z_k within the statistical fluctuations.

The local thermal equilibrium can be demonstrated from MC simulations by calculating the local configurational tem-

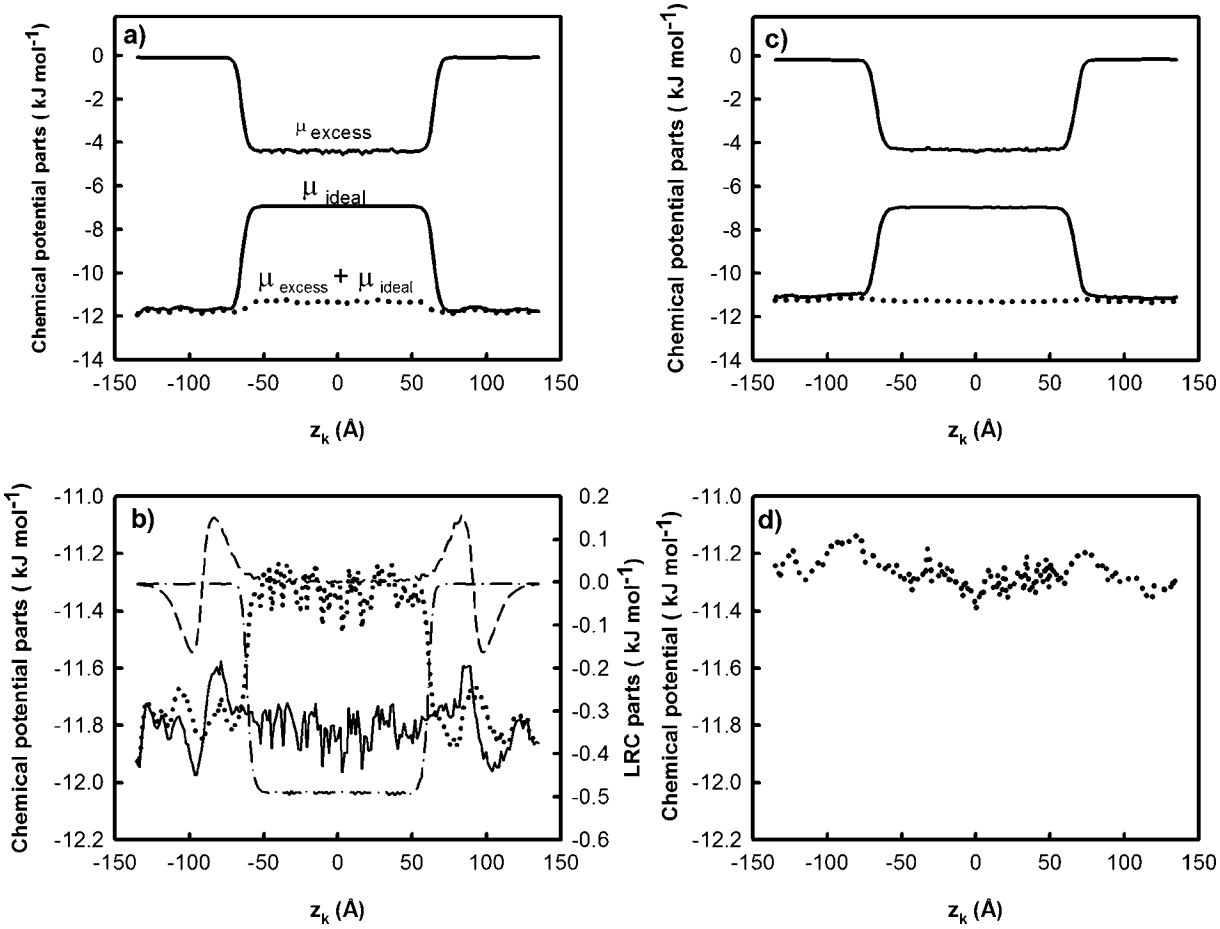

FIG. 3. (a) and (b) Parts of the local chemical potential (kJ mol^{-1}) resulting from MC simulations of methane at $T=120$ K using a truncated LJ potential. (a) Solid line: excess and ideal contributions as indicated in the figure. Dotted line: sum of the excess and ideal parts. (b) Dot-dashed line: first part of the long-range correction to the chemical potential. Dashed line: second part of the tail correction of the chemical potential. Solid line: total chemical potential expressed as $\mu=\mu_{\text{excess}}+\mu_{\text{ideal}}+\mu_{1,\text{LRC}}+\mu_{2,\text{LRC}}$ Dotted line: sum of the excess and ideal parts. (c) and (d) Parts of the local chemical potential calculated from MC simulations using a modified LJ potential via a cubic spline. Solid line: excess and ideal contributions as indicated in the figure. Dotted line: sum of the excess and ideal parts.

perature. Figure 4(a) shows a profile of $T_{\text{conf}}(z_k)$ for the simulation of methane at $T=150$ K. We observe that the local temperature in the liquid and vapor regions matches very well with the Boltzmann temperature. The average temperature calculated over the slabs in the liquid region is 149.8 ± 0.3 K whereas it is equal to 150 ± 5 K in the vapor phases. The increase of the standard deviation in the vapor phases is essentially attributed to the statistics resulting from a smaller number of molecules. In fact, these fluctuations decreases as the temperature and the number of MC cycles increase.

Concerning the mechanical equilibrium, we have already established in previous papers [2,12] that the inclusion of the long-range corrections to the calculation of the components of the pressure tensor led to the constancy of the normal component $p_N(z_k)$ of the pressure tensor with respect to z_k in the liquid and vapor phases. We also showed that the tangential part of the pressure tensor $p_T(z_k)$ was equal to $p_N(z_k)$ in the liquid and vapor regions and exhibited two negative peaks in the interfacial regions. The appropriate long-range corrections to the Irving-Kirkwood (IK) definition of the normal and tangential components of the pressure tensor have been derived by Guo and Lu [20] and are composed of two parts as expressed in Eqs. (34) and (35):

$$p_{N,\text{LRC}}(z_k) = p^{(1)}_{N,\text{LRC}}(z_k) + p^{(2)}_{N,\text{LRC}}(z_k)$$
$$= -\frac{2\pi}{3}\rho^2(z_k)\int_{r_c}^{\infty} dr r^3 \frac{d\mathcal{U}_{\text{LJ},m}(r)}{dr} - \pi\rho(z_k)\int_{r_c}^{\infty} dr$$
$$\times \int_{-r}^{r} d\Delta z[\rho(z)-\rho(z_k)]\frac{d\mathcal{U}_{\text{LJ},m}(r)}{dr}(\Delta z)^2. \quad (34)$$

As concerns the tangential pressure, only the second term is modified and is expressed by

$$p^{(2)}_{T,\text{LRC}}(z_k) = -\frac{\pi}{2}\rho(z_k)\int_{r_c}^{\infty} dr \int_{-r}^{r} d\Delta z[\rho(z)$$
$$-\rho(z_k)]\frac{d\mathcal{U}_{\text{LJ},m}(r)}{dr}[r^2-(\Delta z)^2]. \quad (35)$$

The first term of $p_{N,\text{LRC}}(z_k)$ and $p_{T,\text{LRC}}(z_k)$ is identical to that used in homogeneous molecular simulations by using a local

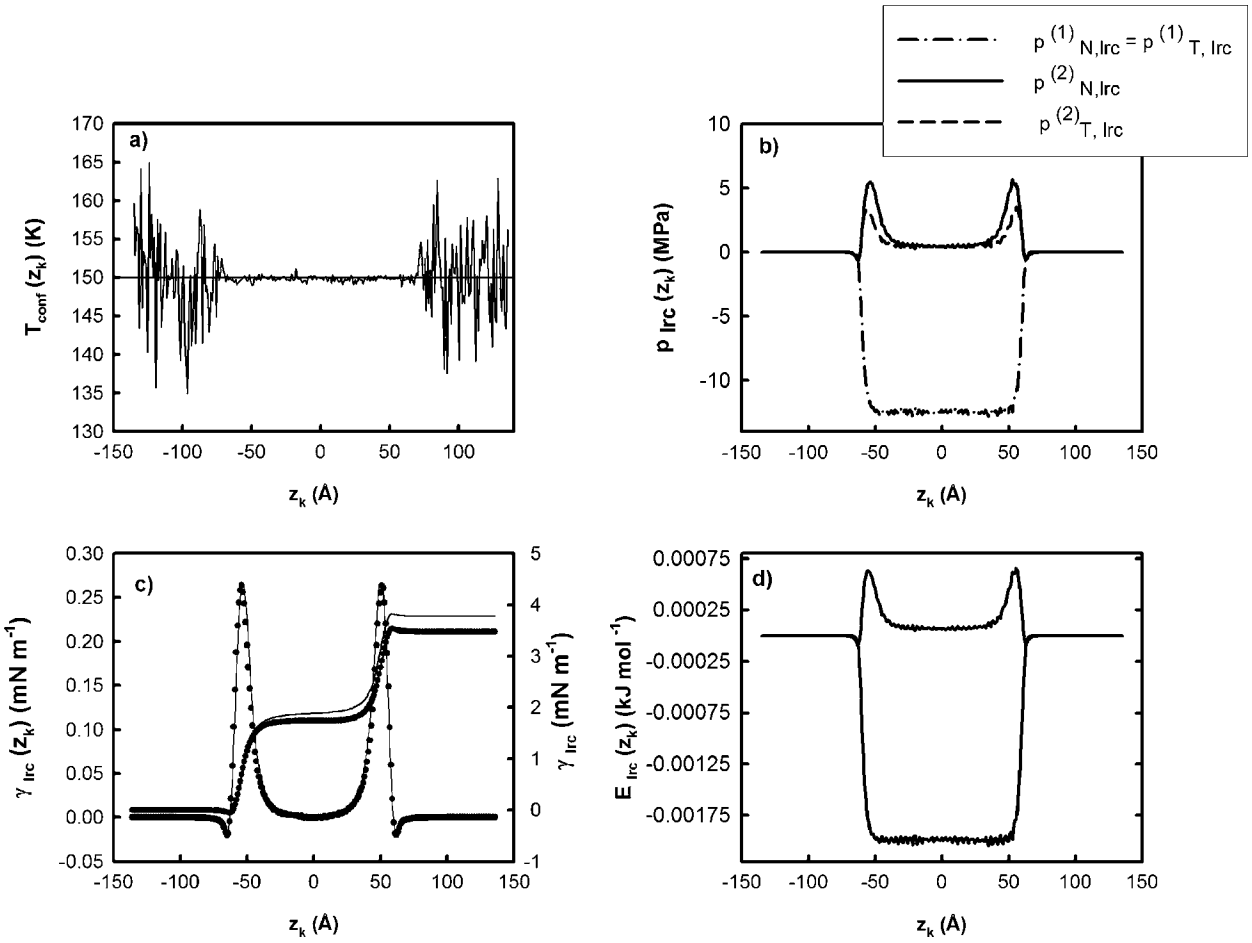

FIG. 4. Thermodynamic properties profiles calculated from MC simulations of methane at 150 K. (a) Configurational temperature. (b) Long-range corrections to the normal and tangential components. (c) Long-range corrections to the surface tension (left axis) calculated from Eqs. (38) and (37) with the corresponding integral (right axis). (d) First and second parts of the long-range corrections to the configurational energy.

density $\rho(z_k)$ whereas the second term takes into account the density differences in the slabs.

We show in Fig. 4(b) the profiles of the long-range corrections to the normal and tangential components of the pressure tensor of the methane at 150 K. We observe that these LRC contributions to the pressure are far from being negligible. The first term of the normal and tangential components can reach −12 MPa in the liquid region. The second terms of p_N and p_T present peaks in the interfacial region with magnitudes between 3 and 5 MPa. The second terms of p_N and p_T can be used to calculate the LRC contribution to the surface tension which essentially results from the integration of the difference between the peaks of p_N and p_T. In fact, the total LRC contribution to the surface tension $\gamma_{\mathrm{IK,LRC}}$ resulting from the IK definition of the pressure components is given by the operational expression

$$\gamma_{\mathrm{IK,LRC}} = \frac{1}{2}\sum_{k=1}^{N_s} \gamma_{\mathrm{IK,LRC}(z_k)} = \frac{1}{2}\sum_{k=1}^{N_s} [p_{N,\mathrm{LRC}}(z_k) - p_{T,\mathrm{LRC}}(z_k)]\delta z, \tag{36}$$

where the term $[p_{N,\mathrm{LRC}}(z_k) - p_{T,\mathrm{LRC}}(z_k)]\delta z$ can be explicitly given by

$$\gamma_{\mathrm{IK,LRC}}(z_k) = \frac{\pi}{2}\rho(z_k)\delta z \int_{r_c}^{\infty} dr \int_{-r}^{r} d\Delta z [\rho(z) - \rho(z_k)] \frac{d\mathcal{U}_{\mathrm{LJ},m}(r)}{dr} [r^2 - 3(\Delta z)^2]. \tag{37}$$

Another operational expression has been developed by Mecke *et al.* [36,37] for the calculation of the profile of the LRC to the surface tension. This expression uses spherical coordinates r and θ and has been recently reformulated for giving the LRC contributions to the pressure tensor components [38]:

$$\gamma_{r\theta,\mathrm{LRC}}(z_k) = \pi \int_{r_c}^{\infty} dr \int_{0}^{\pi} d\theta (1 - 3\cos^2\theta) \frac{d\mathcal{U}_{\mathrm{LJ},m}(r)}{dr} \times \rho(z_i + r\cos\theta)\sin\theta. \tag{38}$$

We observe in Fig. 4(c) that the profiles resulting from the two expressions [Eqs. (37) and (38)] cannot be distinguished. We check that the two profiles present bulk regions where the LRC part is zero and the corresponding integral is flat.

TABLE II. Long-range corrections (mN m^{-1}) to the surface tension calculated from different operational expressions in the cases of methane, *n*-pentane, and *n*-decane.

T (K)	$\gamma_{0,\mathrm{LRC}}$[a]	$\gamma_{\mathrm{Buff,LRC}}$[b]	$\gamma_{r\theta,\mathrm{LRC}}$[c]	$\gamma_{\mathrm{IK,LRC}}$[d]	$\gamma_{\mathrm{TA,LRC}}$[e]
			methane		
120	4.20	3.64	3.45	3.75	2.64
135	3.69	2.95	2.83	3.11	2.20
155	3.01	2.00	1.91	2.15	1.60
170	2.42	1.22	1.20	1.39	1.10
			n-pentane		
300	6.38	5.43	5.29	5.57	4.14
350	5.29	3.80	3.82	4.11	3.16
370	4.77	3.15	3.27	3.52	2.75
400	4.08	2.14	2.42	2.62	2.04
420	3.41	1.45	1.82	1.95	1.54
			n-decane		
450	5.47	4.20	4.31	4.34	3.79
470	5.14	3.61	3.85	3.85	3.30
510	4.16	2.42	2.87	2.80	2.63

[a]Equation (40).
[b]Equation (39).
[c]Equation (38).
[d]Equation (36).
[e]Equation (49).

It means that the system presents a fully developed liquid region and two interfaces with any interaction between them. The profiles show two identical positives peaks at the interface regions and two small negative peaks on the gas side of the surface. The total long-range corrections reported in Table II results from the sum over all slabs and are divided by 2 to take into account the two interfaces of the system. The values calculated from the IK operational expression are slightly greater than those calculated from Eq. (38).

Concerning the Buff expression for the surface tension, specific long-range corrections have been developed by Blokhuis *et al.* [39] and successfully applied in molecular systems [12,33]. This expression is based upon the approximation that the radial distribution function is equal to unity for r greater than the cutoff radius and that the density profile can be fitted to a hyperbolic tangent. This expression takes the form

$$\gamma_{\mathrm{Buff,LRC}} = \frac{\pi}{2}(\rho_l - \rho_v)^2 \int_0^1 ds \int_{r_c}^{+\infty} dr \coth\left(\frac{2rs}{d}\right) \frac{d\mathcal{U}_{\mathrm{LJ},m}(r)}{dr} \times r^4(3s^3 - s), \tag{39}$$

where d is an estimation of the thickness of the interface and s is a parameter defined as $s=(z_i-z_j)/r_{ij}$.

Another expression [40] considers as negligible the vapor density ρ_g and the interface width. This expression takes the form

$$\gamma_{0,\mathrm{LRC}} = \frac{\pi}{8}\rho_l^2 \int_{r_c}^{\infty} dr r^4 \frac{d\mathcal{U}_{\mathrm{LJ},m}(r)}{dr}, \tag{40}$$

where ρ_l is the liquid density. As expected from the initial approximations, the tail correction to the surface tension given by Eq. (40) is overestimated compared to the values resulting from the other methods (Table II). We check that the values resulting from profiles calculed from Eqs. (37) and (38) match very well with that calculated from the Buff expression. The differences between these values are within the statistical fluctuations of the surface tension calculation. To this point, we underline that it is crucial to associate the appropriate expression of the tail contribution when a calculation of the intrinsic surface tension is required.

Using the test-area method, the calculation of the surface tension is carried out in the direct and reverse directions. The calculation of the direct direction involves an increase of the surface area such that $A^{(1)}=A^{(0)}+\Delta A_\epsilon$ whereas a decrease of the surface area is performed in the reverse path as $A^{(-1)}=A^{(0)}-\Delta A_\epsilon$. The surface tension value is averaged over the two directions as $(\gamma_\mathrm{D}+\gamma_\mathrm{I})/2$ where γ_D and γ_I are expressed as $-\frac{k_BT}{2\Delta A_\epsilon}\ln\left\langle\exp\left(-\frac{\Delta\mathcal{U}_{(0\to1)}}{k_BT}\right)\right\rangle_0$ and $-\frac{k_BT}{2\Delta A_\epsilon}\ln\left\langle\exp\left(-\frac{\Delta\mathcal{U}_{(0\to-1)}}{k_BT}\right)\right\rangle_0$, respectively. The perturbation of the box dimensions is performed over the configurations of the reference state and leads to virtual configurations of the perturbed state. The ensemble average is carried out over the reference system and the virtual configurations of the perturbed system do not participate to the Markov chain of states. In this sense, it is closely related to Widom's method [19] for the calculation of the chemical potential for which the perturbation leads to the insertion of a virtual particle.

Table III shows the surface tension calculated from the TA method in the direct and the reverse directions for methane, *n*-pentane, and *n*-decane. We check that the value of ϵ

TABLE III. Surface tension (mN m^{-1}) calculated from the test-area (TA) method in the direct and inverse directions with the corresponding long-range corrections.

	γ_{TA} [a]			$\gamma_{TA,LRC}$ [b]		
T (K)	γ_D	γ_I	γ	$\gamma_{D,LRC}$	$\gamma_{I,LRC}$	γ_{LRC}
			methane			
120	10.43	10.74	10.59	2.61	2.67	2.64
135	7.93	7.52	7.73	2.20	2.20	2.20
155	4.50	4.65	4.58	1.50	1.63	1.60
170	2.72	2.38	2.55	1.09	1.11	1.10
			n-pentane			
300	13.40	13.88	13.64	4.01	4.28	4.14
350	8.05	8.12	8.09	2.98	3.35	3.16
370	6.00	6.15	6.07	2.59	2.92	2.75
400	4.57	4.50	4.54	1.98	2.11	2.04
420	3.01	3.04	3.03	1.48	1.59	1.54
			n-decane			
450	7.55	7.90	7.72	3.38	4.20	3.79
470	6.13	6.44	6.29	2.81	3.80	3.30
510	2.77	2.76	2.76	2.36	2.91	2.63

[a]Equation (24).
[b]Equation (49).

used (5×10^{-4}) is appropriated for an accurate calculation of γ_{TA} with a small deviation between the forward and backward directions. We also check that this method can be easily extended to molecular systems. To complete the calculation of the surface tension using the TA formalism, we use the statistical mechanical perturbation theory developed by Zwanzig in 1954 [41] where the exponential and the logarithm of Eq. (23) can be expanded in powers of $1/T$ at high temperatures to give the following operational expression of the surface tension:

$$\gamma = -\frac{1}{\Delta A_\epsilon}\left(\langle\Delta\mathcal{U}\rangle - \frac{\langle\Delta\mathcal{U}^2\rangle - \langle\Delta\mathcal{U}\rangle^2}{2k_BT} + \frac{\langle\Delta\mathcal{U}^3\rangle - 3\langle\Delta\mathcal{U}^2\rangle\langle\Delta\mathcal{U}\rangle + 2\langle\Delta\mathcal{U}\rangle^3}{6k_B^2T^2}\right) + O\left(\frac{1}{k_BT}\right)^2, \tag{41}$$

where $\Delta\mathcal{U}$ is calculated as the half sum of $\Delta\mathcal{U}_{(0\to1)}$ and $\Delta\mathcal{U}_{(0\to-1)}$. Using this expression, we check that the surface tensions are strictly identical to those calculated from Eq. (23).

Figure 5(a) shows the profiles of the γ_{TA} surface tension calculated in the two directions. The two profiles are very close and the total values of γ_{TA} resulting from the arithmetic sum of the local value of each slab correspond exactly to those calculated from Eq. (23). This result confirms the validity of the local operational expression of $\gamma_{TA}(z_k)$.

Throughout this paper, we propose to establish the operational expression for the long-range correction to the surface tension based upon the TA technique. To do so, let us recall that the LRC to the configurational energy [20] is given by

$$\mathcal{U}_{LRC}(z_k) = \mathcal{U}^{(1)}_{LRC}(z_k) + \mathcal{U}^{(2)}_{LRC}(z_k) = 2\pi\rho^2(z_k)V_s\int_{r_c}^{\infty} drr^2\mathcal{U}_{LJ,m}(r) + \pi\rho(z_k)V_s\int_{r_c}^{\infty} dr\int_{-r}^{r} d\Delta z[\rho(z)-\rho(z_k)]r\mathcal{U}_{LJ,m}(r). \tag{42}$$

This LRC contribution is constituted of two terms, one depending on the local density and the second taking into account the differences in density between the slabs. The two terms are represented in Fig. 4(d). The shape of the profile of the LRC to the configurational energy is very close to that of the pressure profile. From the TA method, we obtain a LRC contribution by writing that the LRC part is different between the total contribution and the intrinsic contribution as in the equations

$$\gamma_{TA,LRC} = \gamma_{TA,tot} - \gamma_{TA} \tag{43}$$

$$= -\frac{k_BT}{2\Delta A_\epsilon}\ln\frac{\left\langle\exp\left(-\frac{(\Delta\mathcal{U}+\Delta\mathcal{U}_{LRC})}{k_BT}\right)\right\rangle}{\left\langle\exp\left(-\frac{\Delta\mathcal{U}}{k_BT}\right)\right\rangle} \tag{44}$$

$$\approx -\frac{k_BT}{2\Delta A_\epsilon}\ln\left\langle\exp\left(-\frac{\Delta\mathcal{U}_{LRC}}{k_BT}\right)\right\rangle. \tag{45}$$

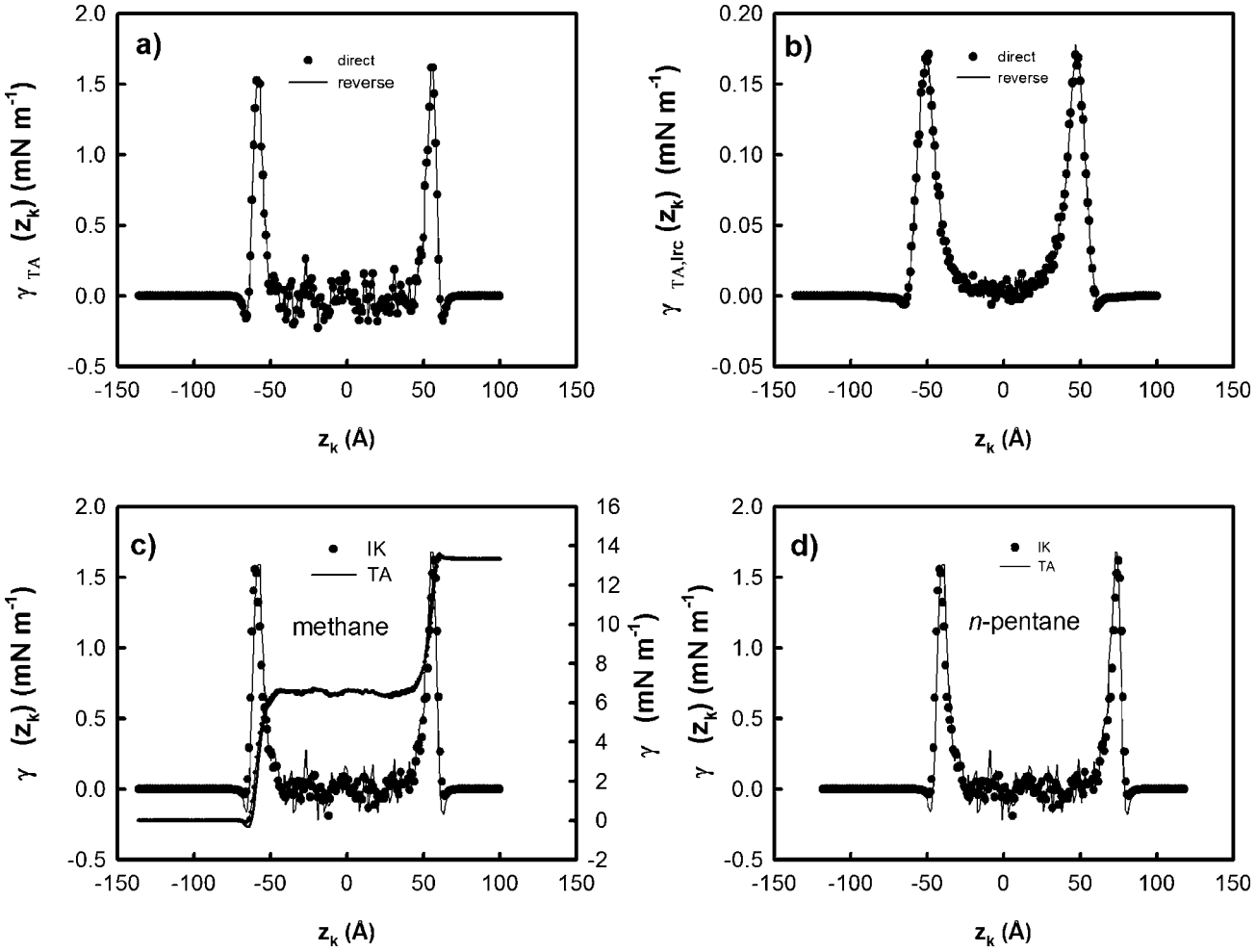

FIG. 5. Surface tension profiles calculated from MC simulations of methane at $T=120$ K calculated in the forward and backward directions using the TA approach. (a) Intrinsic surface tension contribution. (b) LRC contribution to the surface tension. Total surface tension calculated using the TA and IK methods from MC simulations of (c) methane with the corresponding integral (right axis) and (d) *n*-pentane.

Expression (45) is obtained by assuming that the two terms $\left\langle \exp\left(-\frac{(\Delta \mathcal{U})}{k_B T}\right)\right\rangle$ and $\left\langle \exp\left(-\frac{(\Delta \mathcal{U}_{\mathrm{LRC}})}{k_B T}\right)\right\rangle$ are independent. The difference between the two averages $\left(\left\langle \exp\left(-\frac{(\Delta \mathcal{U}+\Delta \mathcal{U}_{\mathrm{LRC}})}{k_B T}\right)\right\rangle\right)$ and $\left\langle \exp\left(-\frac{(\Delta \mathcal{U})}{k_B T}\right)\right\rangle\left\langle \exp\left(-\frac{(\Delta \mathcal{U}_{\mathrm{LRC}})}{k_B T}\right)\right\rangle$ is within 10^{-6} units. This result shows that Eq. (45) reasonably represents an appropriate operational expression for the LRC part of the surface tension calculated from the TA approach.

The local long-range corrections contribution the surface tensions calculated from the TA approach are established by assuming that the terms $\left\langle \exp\left(-\frac{(\Delta \mathcal{U}_{z_k})}{k_B T}\right)\right\rangle_{z_k}$ and $\left\langle \exp\left(-\frac{(\Delta \mathcal{U}_{\mathrm{LRC},z_k})}{k_B T}\right)\right\rangle_{z_k}$ are uncorrelated for each z_k. We check this assumption by calculating the local spatial correlation function $C(z_k)$ defined by the difference between $\left\langle \exp\left(-\frac{(\Delta \mathcal{U}_{z_k}+\Delta \mathcal{U}_{\mathrm{LRC},z_k})}{k_B T}\right)\right\rangle_{z_k}$ and $\left\langle \exp\left(-\frac{(\Delta \mathcal{U}_{z_k})}{k_B T}\right)\right\rangle_{z_k}$ $\times\left\langle \exp\left(-\frac{(\Delta \mathcal{U}_{\mathrm{LRC},z_k})}{k_B T}\right)\right\rangle_{z_k}$. This curve shows in Fig. 1(b) local differences less than 10^{-6} unit and justifies the fact of decomposing the local surface tension resulting from the TA method into an intrinsic local contribution and a tail local contribution. The local expression of the LRC of the TA method derived from expression (46) is thus given by

$$\gamma_{\mathrm{TA,LRC}} = -\frac{k_B T}{2\Delta A_\epsilon} \ln\left\langle \exp\left(-\frac{(\mathcal{U}^{(1)}_{\mathrm{LRC}} - \mathcal{U}^{(0)}_{\mathrm{LRC}})}{k_B T}\right)\right\rangle_0, \quad (46)$$

where $\mathcal{U}^{(1)}_{\mathrm{LRC}}$ and $\mathcal{U}^{(0)}_{\mathrm{LRC}}$ represent the sums over the slabs of $\mathcal{U}_{\mathrm{LRC}}(z_k')$ and $\mathcal{U}_{\mathrm{LRC}}(z_k)$, respectively:

$$\gamma_{\mathrm{TA,LRC}}(z_k) = -\frac{k_B T}{\Delta A_\epsilon} \ln\left\langle \exp\left(-\frac{[\mathcal{U}^{(1)}_{\mathrm{LRC}}(z_k') + \mathcal{U}^{(2)}_{\mathrm{LRC}}(z_k')] - [\mathcal{U}^{(1)}_{\mathrm{LRC}}(z_k) + \mathcal{U}^{(2)}_{\mathrm{LRC}}(z_k)]}{k_B T}\right)\right\rangle_0. \quad (47)$$

TABLE IV. Different contributions of surface tension values ($mN\,m^{-1}$) calculated from different operational expressions for methane, *n*-pentane, and *n*-decane. The experimental surface tension are given for comparison.

	γ_{Buff}		γ_{IK}		γ_{TA}					
T (K)	γ [a]	γ_{LRC} [b]	γ [c]	γ_{LRC} [d]	γ [e]	γ_{LRC} [f]	$\gamma_{Buff,tot}$	$\gamma_{IK,tot}$	$\gamma_{TA,tot}$	γ_{expt}
					methane					
120	9.5_{12}	3.6_{1}	9.5_{12}	3.8_{1}	10.6_{12}	2.6_{1}	13.1_{13}	13.3_{13}	13.2_{12}	11.3
135	6.8_{13}	2.9_{1}	6.8_{13}	3.1_{1}	7.7_{13}	2.2_{1}	9.8_{14}	10.0_{14}	9.9_{13}	8.0
155	4.0_{8}	2.0_{1}	4.0_{8}	2.2_{1}	4.6_{9}	1.6_{1}	6.0_{8}	6.2_{8}	6.2_{10}	4.3
170	2.2_{7}	1.2_{1}	2.2_{7}	1.4_{1}	2.5_{7}	1.1_{1}	3.4_{8}	3.6_{8}	3.6_{8}	2.1
					n-pentane					
300	12.0_{19}	5.4_{1}	12.0_{19}	5.6_{1}	13.6_{19}	4.1_{1}	17.4_{20}	17.6_{19}	17.8_{19}	15.3
350	7.0_{25}	3.8_{1}	7.0_{25}	4.1_{3}	8.1_{24}	3.2_{1}	10.8_{25}	11.1_{25}	11.2_{24}	10.0
370	5.1_{13}	3.2_{1}	5.1_{13}	3.5_{3}	6.1_{12}	2.7_{2}	8.3_{13}	8.7_{13}	8.8_{14}	8.0
400	3.9_{14}	2.1_{1}	3.9_{14}	2.6_{2}	4.5_{14}	2.0_{2}	6.0_{14}	6.6_{15}	6.6_{14}	5.1
420	2.6_{16}	1.4_{1}	2.6_{16}	2.0_{1}	3.0_{15}	1.5_{1}	4.1_{16}	4.6_{16}	4.6_{15}	3.4
					n-decane					
450	6.0_{22}	4.2_{1}	6.0_{22}	4.3_{1}	7.7_{24}	3.8_{2}	10.2_{23}	10.3_{23}	11.5_{25}	10.4
470	4.8_{25}	3.6_{1}	4.8_{25}	3.8_{3}	6.3_{25}	3.3_{4}	8.4_{25}	8.7_{25}	9.6_{28}	8.8
510	1.7_{16}	2.4_{1}	1.7_{16}	2.8_{2}	2.8_{16}	2.6_{2}	4.2_{15}	4.5_{16}	5.4_{17}	5.9

[a]Equation (29).
[b]Equation (39).
[c]Equation (28).
[d]Equation (36).
[e]Equation (24).
[f]Equation (49).

The difference in Eq. (47) between the terms $\mathcal{U}^{(1)}_{LRC}(z'_k)$ and $\mathcal{U}^{(1)}_{LRC}(z_k)$ vanishes because the transformation conserves the local density in the perturbed state. The second term depends on $d\Delta z$. As a consequence, it is changed by the perturbation. It means that the double integral of the second term is different in the two states. This difference in the second terms gives the tail correction of the surface tension calculated from the TA method. This LRC part is expressed by

$$\gamma_{TA,LRC}(z_k) = -\frac{k_B T}{\Delta A_\epsilon} \ln\left\langle \exp\left(-\frac{(\mathcal{U}^{(2)}_{LRC}(z'_k) - \mathcal{U}^{(2)}_{LRC}(z_k))}{k_B T}\right)\right\rangle_0. \tag{48}$$

The total long-range correction for the simulation is then calculated according

$$\gamma_{TA,LRC} \approx \frac{1}{2}\sum_{i=1}^{N_s} \gamma_{TA,LRC}(z_k), \tag{49}$$

where N_s is the total number of slabs in the simulation box. This expression supposes that the local long-range correction parts of the slabs of z_k and z_{k+1} tension are independent. This uncorrelation was already established for the intrinsic surface tension in Eq. (24) and can be extended to the local LRC contribution of the surface tension. The LRC contributions to the surface tension are reported in Table II for the direct and reverse directions. We observe small deviations between the two directions, indicating a good stability of the perturbation algorithm. Using the TA method and a cutoff radius of 12 Å, we show that the tail correction of the surface tension represents between 20% and 50% of the total value depending on both temperature and alkane chain length. The profiles of this tail contribution are shown in Fig. 5(b). In line with the LRC values given in Table III, we find that the profiles are similar in the two directions. The value calculated from Eq. (46) and the value resulting from the profiles are rigorously identical. Table II also shows that the long-rang corrections to the surface tension calculated by the test-area method are smaller than those calculated from IK [Eq. (36)], Buff [Eq. (29)], and Mecke [Eq. (38)] methods. The difference between the LRC contributions calculated by the IK and TA methods decreases significantly as the temperature increases.

The total surface tension values are reported in Table IV with their corresponding long-range corrections. Interestingly, we observe that the total values calculated using the IK, Buff, and TA methods match very well with the standard deviations. It means that once the appropriated LRC correction is applied, the total surface tension is not dependent on the method used. The profiles of the total surface tension resulting from IK and TA calculations are shown in Fig. 5(c) for methane and can be considered as very close. We only observe a small difference in the magnitude of the small negative peaks on the vapor side of the interface which is greater for the TA than for the IK method. We observe that the interface region is characterized by strongly negative values of the tangential component of the pressure, indicating that the liquid in this region is under tension. We also see that the region close the surface at the vapor side is characterized

by small positive values of this pressure tangential part, suggesting a compression of this zone on the vapor side. The presence of this negative peak on the vapor side of the interface has been subjected to controversial discussions and depends on the method used for the calculation of the pressure tensor [6,42]. The TA method confirms the presence of these small negative peaks by using the energy change for the expression of the surface tension. The shape and the final value of the integral of each profiles (right axis) are the same for the IK and TA methodologies. The same features can be observed for the profiles of the total surface tension of alkane chains [see Fig. 5(d)].

To investigate further the TA calculation, we observe in Table IV that the intrinsic surface tension without a LRC contribution calculated with the TA method is larger than that calculated from IK and Buff expressions. The fact that the total value of the surface tension is the same for the TA and IK methods means that the LRC part of the surface tension calculated from the TA and IK methods follows the opposite trend. The IK and Buff expressions use the derivative of the potential to express the surface tension whereas the TA method only uses the potential. We have already shown [2] that the truncated force does not correspond to the truncated potential due to the fact that the truncated potential is not differentiable at the cutoff value. This effect is much more marked in simulation of two-phase systems, which exhibit nonuniformity of the density distribution along the axis perpendicular to the surface. We have underlined that the MD simulation using a truncated force does not yield the same coexisting densities and interfacial properties than the MC simulation using a truncated potential. The two methods lead to the same results under the condition that the potential used be differentiable at the cutoff value. To underline this point, we have performed MC simulations of the methane using a LJ potential changed by a cubic spline potential defined in Eq. (32). In such a simulation, both the potential and its derivative are continuous at the cutoff value. As the potential and force are zero at the cutoff, the calculated properties do not need to be corrected. These simulations do not aim to yield results in close agreement with experiments but to numerically highlight some features. We compare the results of surface tension of methane calculated from TA, IK, and Buff expressions for MC simulations using both a truncated LJ potential and a LJ potential modified by a cubic spline function (see Table V). As expected from the equivalence between γ_{TA} and the macroscopic definition of γ (Appendix A), the different operational expressions provide exactly the same values for the surface tension when the potential is differentiable at the cutoff. The profiles resulting from IK and TA methods shown in Fig. 6 can be considered as close. However, we detect a slight difference between the profiles of the surface tension calculated from the TA and IK approaches at the interfacial region. We note that the profiles resulting from the TA approach present small peaks slightly more negative than those resulting from the IK definition at the inferface [Figs. 5(c) and 6]. The total values resulting from the integration of the profiles are not affected by this feature and are identical for the IK and TA methods.

We confirm what we have already demonstrated in a previous paper [2]. The impulsive contribution to the force due to the discontinuity of the potential at the cutoff radius can be ignored when the potential is differentiable at the cutoff distance. In this case, the TA and IK techniques are rigorously identical. If we follow the strategy of Trokhymchuk and Alejandre [1] consisting in adding a δ function in the definition of the force to take into account this impulsive contribution to the pressure, we find that the new value calculated from the IK method is increased and comparable with that calculated using the TA method according to the values of γ (mN m^{-1}) for methane at 150 K ($\gamma_{IK}=6.8_{13}$, $\gamma_{TA}=7.7_{13}$, $\gamma_{IK+\delta}=7.7_{13}$). This result is in line with our previous MC simulations using different potentials [2]. We also observe that the difference between the IK and TA methods decreases as the temperature increases. It means that the discrepancy between the TA and IK methods decreases when the difference of density between the two phases is attenuated in line with the fact that the discontinuity of the potential at the cutoff value plays a significant role especially as the density gradient is marked.

Following the perturbation formalism, we try to calculate a local entropy change in the liquid-vapor surface. The local

TABLE V. Surface tension of methane (mN m^{-1}) resulting from MC simulations using a truncated LJ potential and a modified LJ potential.

			γ_{TA}[c]		
T (K)	γ_{Buff}[a]	γ_{IK}[b]	γ_D	γ_I	γ
Truncated LJ potential					
120	9.49	9.50	10.43	10.74	10.59
135	6.83	6.88	7.93	7.52	7.73
150	4.76	4.78	5.34	5.49	5.42
Cubic spline modified LJ potential[d]					
120	8.54	8.54	8.52	8.58	8.55
135	5.48	5.48	5.50	5.47	5.48
150	3.02	3.08	3.03	3.03	3.03

[a]Equation (29).
[b]Equation (28).
[c]Equation (23).
[d]Equation (32).

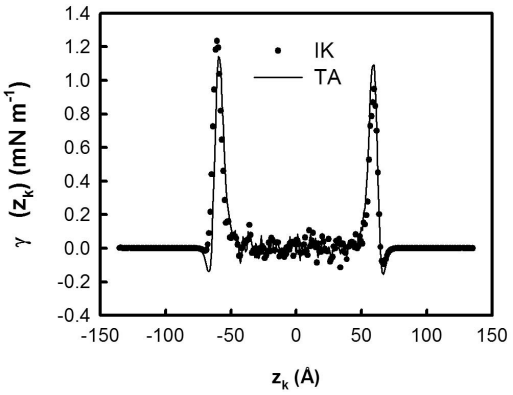

FIG. 6. Total surface tension profiles calculated from MC simulations of methane at $T=120$ K using a LJ potential changed by the addition of a cubic spline.

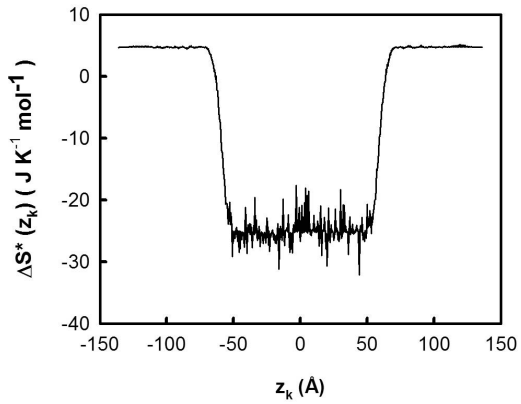

FIG. 7. Local entropy profiles calculated from MC simulations of methane at $T=120$ K.

operational expression of the local entropy is derived in Eq. (B4) of Appendix B. To compare this property with an experimental value, we use the $\Delta\mu^*$ defined by Ben-Naim and Marcus [43] as

$$\Delta\mu^* = \mu_l^* - \mu_g^* = -k_B T \ln\left(\frac{\rho_l}{\rho_v}\right), \tag{50}$$

where ρ_g and ρ_l are the number density of the liquid and vapor phases, respectively:

$$\Delta S^* = (S_l^{N+1} - S_l^N)^* - (S_g^{N+1} - S_g^N)^* = \langle \Delta S_{z_k}^* \rangle_l - \langle \Delta S_{z_k}^* \rangle_g = -\frac{\partial \Delta\mu^*}{\partial T}. \tag{51}$$

The calculation of the averages of $\langle \Delta S_{z_k}^* \rangle_l$ and $\langle \Delta S_{z_k}^* \rangle_v$ is performed over the slabs of the liquid and vapor phases, respectively. This calculation required a grid of (100×100) ghost particles inserted at each 1.0 Å. The average has been carried out over 20 000 configurations constituted of 3000 molecules of methane at $T=120$ K. The corresponding total CPU time is about 312 days on a single processor and has been reduced to 15 CPU days by using 26 processors at a time. The profile of the local excess entropy variation is shown in Fig. 7. The average values of the local excess entropy change is 4.7 J K^{-1} mol^{-1} and −25.0 J K^{-1} mol^{-1} for the liquid and vapor regions, respectively. This leads to a value of −29.7 J K^{-1} mol^{-1} for ΔS^* whereas the value calculated from the derivative of μ^* with respect to the temperature is equal to −29.2 J K^{-1} mol^{-1}. Our calculation agrees quantitatively well with the experimental data available. It proves the efficiency of the sampling and the feasibility of calculating the excess entropy part for a two-phase system.

VI. CONCLUSIONS

This work lies within the framework of the molecular simulations of two-phase systems where the nonuniformity of the density distribution along the direction normal to the interface requires one to pay attention to the calculation of the interfacial properties and their long-range corrections as well as the truncation procedures. One of our objectives is to use a relatively small cutoff for the simulation of the two-phase systems in order to make the direct simulations competitive with the GEMC simulations. In this case, the use of LRC contributions is required.

We have focused on the calculation of the profile of the chemical potential along the axis perpendicular to the surface. We have used a modified version of the Widom technique adapted to heterogenous systems. We have highlighted the importance of the long-range corrections to be added to the chemical potential. For a MC simulation using a truncated LJ potential, we have shown that the chemical potential profile is uniform when two long-range corrections are included in the calculation. For a MC simulation using a LJ potential changed by a switching function that makes the first and second derivatives of the potential continuous at the cutoff distance, it has been established that the profile of the sum of the ideal and excess parts is constant throughout the simulation box.

The different operational expressions (IK, TA, Buff) for the calculation of the surface tension with their corresponding LRC expressions have been presented. We have tested the novel technique called the "test-area" method on MC simulations of methane and applied it to the calculation of surface tension of alkanes such as *n*-pentane and *n*-decane. We have established the expression of the surface tension profile from the TA approach and demonstrated the LRC expressions resulting from this perturbation method. All the operational expressions of the surface tension give similar results once the appropriate LRC contributions are included. The difference between the TA and IK methods has been explained by the discontinuity of the potential at the cutoff distance. We have removed this discontinuity by using LJ interactions truncated via a polynomial function and shown that the TA and IK approaches lead to the same value of the surface tension.

This work has been completed by the calculation of the local entropy change in the liquid-vapor interface of the methane. The calculation of this property represents a challenge at the CPU level and the comparison of this property with experimental data is very satisfactory.

APPENDIX A: SURFACE TENSION

1. Thermodynamic route and virial expression

Let us return to Eq. (22) and express the exponential of $\mathcal{U}^{(1)}(\mathbf{r}'^N)$ as a Taylor expansion [Eq. (A1)] about the point $\mathbf{r}$ up to the second order where $O((\mathbf{r}'_{ij}-\mathbf{r}_{ij})^2)$ represent second- and higher-order terms. For clarity, the demonstration is only given for a system of N particles. The molecular version of the expression given in Eq. (A6) is expressed by Eq. (29):

$$\exp\left(-\frac{\mathcal{U}^{(1)}(\mathbf{r}'^N)}{k_B T}\right) = \exp\left(-\frac{\mathcal{U}^{(0)}(\mathbf{r}^N)}{k_B T}\right)\left[1 - \frac{1}{k_B T}\sum_{i=1}^{N-1}\sum_{j=i+1}^{N} \times (\mathbf{r}'_{ij}-\mathbf{r}_{ij})\frac{d\mathcal{U}^{(0)}(r_{ij})}{dr_{ij}}\right] + O((\mathbf{r}'_{ij}-\mathbf{r}_{ij})^2). \tag{A1}$$

Replacing $\mathcal{U}^{(1)}(\mathbf{r}'^N)$ in Eq. (22) by the right term of Eq. (A1) leads to the expressions given in Eqs. (A2) and (A3):

$$\gamma = -\frac{k_B T}{\Delta A_\epsilon} \ln \frac{\int d\mathbf{r}^N \left[1 - \frac{1}{k_B T} \sum_{i=1}^{N-1} \sum_{j=i+1}^{N} (\mathbf{r}'_{ij} - \mathbf{r}_{ij}) \frac{d\mathcal{U}^{(0)}(r_{ij})}{dr_{ij}} \right] \exp\left(-\frac{\mathcal{U}^{(0)}(\mathbf{r}^N)}{k_B T} \right)}{\int d\mathbf{r}^N \exp\left(-\frac{\mathcal{U}^{(0)}(\mathbf{r}^N)}{k_B T} \right)} \tag{A2}$$

$$= -\frac{k_B T}{\Delta A_\epsilon} \ln \left\langle 1 - \frac{1}{k_B T} \sum_{i=1}^{N-1} \sum_{j=i+1}^{N} (\mathbf{r}'_{ij} - \mathbf{r}_{ij}) \frac{d\mathcal{U}^{(0)}(r_{ij})}{dr_{ij}} \right\rangle. \tag{A3}$$

Let us expand the position vector $\mathbf{r}'_{ij}$ in the perturbed system in powers of ϵ such as

$$\mathbf{r}'_{ij} = \mathbf{r}_{ij} \left[1 + \frac{\epsilon}{2} \left(1 - \frac{3z_{ij}^2}{r_{ij}^2} \right) \right] + O(\epsilon^2), \tag{A4}$$

where $O(\epsilon^2)$ contain second- and higher-order terms. The incorporation of the second term of Eq. (A4) into Eq. (A3) allows one to obtain an intermediate expression [Eq. (A5)] for the surface tension within the perturbation methodology. By applying a first-order Taylor series to the expression of the logarithm in Eq. (A5) and dividing by 2 to take into account the specificity of the system, we obtain a new expression given in Eq. (A6) which takes the advantage to be solely calculated in the reference system:

$$\gamma = -\frac{k_B T}{2\Delta A_\epsilon} \ln \left\langle 1 - \frac{\epsilon}{k_B T} \sum_{i=1}^{N-1} \sum_{j=i+1}^{N} \frac{\mathbf{r}_{ij} \cdot \mathbf{r}_{ij} - 3z_{ij} z_{ij}}{2r_{ij}} \frac{d\mathcal{U}^{(0)}(r_{ij})}{dr_{ij}} \right\rangle_0 \tag{A5}$$

$$= \frac{1}{2A} \left\langle \sum_{i=1}^{N-1} \sum_{j=i+1}^{N} \frac{\mathbf{r}_{ij} \cdot \mathbf{r}_{ij} - 3z_{ij} z_{ij}}{2r_{ij}} \frac{d\mathcal{U}^{(0)}(r_{ij})}{dr_{ij}} \right\rangle_0. \tag{A6}$$

This expression has already been established by Salomons and Mareschal [40]. As was underlined by several authors [3,8,40], this expression is consistent with that resulting from the mechanical definition of the surface tension of a planar surface. In this latter, γ is expressed as the product of the L_z dimension and the difference between the normal and tranverse components of the pressure.

2. Equivalence between γ_{TA} and γ

The normal and tangential components of the pressure can be expressed within the grand canonical ensemble (μVT) by using the equations

$$p_N = p_{zz} = -\left(\frac{\partial \Omega}{\partial V} \right)_{\mu,T,L_x,L_y} = -\left(\frac{\partial \Omega}{\partial L_z} \frac{\partial L_z}{\partial V} \right)_{\mu,T,L_x,L_y}$$

$$= -\frac{1}{A} \left(\frac{\partial \Omega}{\partial L_z} \right)_{\mu,T,L_x,L_y}, \tag{A7}$$

$$p_{xx} = -\left(\frac{\partial \Omega}{\partial V} \right)_{\mu,T,L_y,L_z} = -\left(\frac{\partial \Omega}{\partial L_x} \frac{\partial L_x}{\partial V} s \right)_{\mu,T,L_y,L_z}$$

$$= -\frac{1}{L_y L_z} \left(\frac{\partial \Omega}{\partial L_x} \right)_{\mu,T,L_y,L_z} \tag{A8}$$

$$= -\frac{1}{L_y L_z} \left(\frac{\partial \Omega}{\partial A} \frac{\partial A}{\partial L_x} \right)_{\mu,T,L_y,L_z} = -\frac{1}{L_z} \left(\frac{\partial \Omega}{\partial A} \right)_{\mu,T,L_z}. \tag{A9}$$

By applying the transformations of Eqs. (A8) and (A9) to p_{yy}, we obtain the following expression for this component:

$$p_{yy} = -\left(\frac{\partial \Omega}{\partial V} \right)_{\mu,T,L_x,L_z} = -\frac{1}{L_z} \left(\frac{\partial \Omega}{\partial A} \right)_{\mu,T,L_z}, \tag{A10}$$

where Ω is the grand potential, T the temperature, V the volume defined as $L_x L_y L_z$, $A = L_x L_y$ the area of the interface, and μ the chemical potential. The normal part of the pressure p_T is the half-sum of the p_{xx} and p_{yy} components. From Eqs. (A9) and (A10), p_T is expressed as $-\frac{1}{L_z}\left(\frac{\partial \Omega}{\partial A}\right)_{\mu,T,L_z}$.

The surface tension γ can be calculated from the macroscopic averages through

$$\gamma = (p_N - p_T)\frac{L_z}{2} = -\frac{L_z}{2} \left[\frac{1}{A} \left(\frac{\partial \Omega}{\partial L_z} \right)_{\mu,T,L_x,L_y} - \frac{1}{L_z} \left(\frac{\partial \Omega}{\partial A} \right)_{\mu,T,L_z} \right]. \tag{A11}$$

By considering the expression

$$\left(\frac{\partial \Omega}{\partial L_z} \right)_{\mu,T,A} \left(\frac{\partial L_z}{\partial A} \right)_{\Omega,\mu,T} \left(\frac{\partial A}{\partial \Omega} \right)_{\mu,T,L_z} = 1, \tag{A12}$$

Eq. (A11) becomes

$$\gamma = -\frac{L_z}{2} \left(\frac{\partial \Omega}{\partial A} \right)_{\mu,T,L_z} \left[\frac{1}{A} \left(\frac{\partial A}{\partial L_z} \right)_{\Omega,\mu,T} - \frac{1}{L_z} \right] \tag{A13}$$

$$= \left(\frac{\partial \Omega}{\partial A} \right)_{\mu,T,L_z} = \left(\frac{\partial \Omega}{\partial A} \right)_{\mu,T,V} \tag{A14}$$

$$= \gamma_{TA}. \tag{A15}$$

Equation (A14) is obtained by considering that $dV = A dL_z + L_z dA = 0$. This is explained by the fact that the perturbation

is carried out at constant volume. By substituting dA/dL_z into Eq. (A13) by $-A/l_z$, we find the expression given in Eq. (A14). For a system with a planar surface, $\Omega(\mu,T,V)$ is equivalent to $\Omega(\mu,T,L_z,A)$. This leads to the right term in Eq. (A14).

When the geometry of the system leads to a nonuniform density distribution along the z direction normal to liquid surface area, we expect there a dependence of the thermodynamic properties only in this direction. We aim to establish a local surface tension $\gamma_{\mathrm{TA}}(z_k)$ comparable to $\gamma_{\mathrm{IK}}(z_k)$. The following demonstration assumes that there is no correlation between two neighboring slabs as is the case within the mean-field approximation. We have shown in Fig. 1 that the two terms $\left\langle \exp\left(-\frac{\Delta \mathcal{U}_{z_k}}{k_B T}\right)\right\rangle_{z_k}$ $\left\langle \exp\left(-\frac{\Delta \mathcal{U}_{z_{k+1}}}{k_B T}\right)\right\rangle_{z_{k+1}}$ can be considered as independent with a local uncorrelation value less than 10^{-5}. This numerical check allows us to define a local surface tension $\gamma_{\mathrm{TA}}(z_k)$ defined from a local grand potential Ω_{z_k}. The existence of the local grand potential is subjected to the fact that there is no correlation between neighboring slabs. Using this approximation, all the slabs can be treated independently.

Let us recall that the simulation box is divided into N_s slabs of width δz and volume V_s. To make the mathematical expressions of the local thermodynamic properties lighter, we replace $\gamma(z_k)$ by γ_{z_k}. The total number of molecules, N, is constant whereas the number of molecules, N_{z_k}, is each slab fluctuates within the simulation. This is equivalent to fix the chemical potential μ_{z_k} of the alkanes at each z_k position. The relevant thermodynamic potential for a slab k is therefore Ω_k defined as $\Omega_{z_k}=U_{z_k}-T_{z_k}S_{z_k}-N_{z_k}\mu_{z_k}$ where U_{z_k} is the energy of the slab k, S_{z_k} its entropy, and μ_{z_k} and N_{z_k} are the chemical potential and the number of molecules of this slab, respectively. The grand potential depending on z_k is directly related to the grand canonical partition function Ξ_{z_k} at z_k via

$$\Omega_{z_k} = -k_B T \ln \Xi_{z_k}, \tag{A16}$$

where Ξ_{z_k} can be expressed as

$$\Xi_{z_k} = \sum_{N=0}^{\infty} \frac{1}{N!\Lambda^{3N}} \exp\left(\frac{\mu_{z_k} N}{k_B T}\right) \int d\mathbf{r}^N \exp\left(-\frac{U_{z_k}(\mathbf{r}^N)}{k_B T}\right). \tag{A17}$$

The local surface tension γ_{z_k} is given by

$$\gamma_{\mathrm{TA},z_k} = \left(\frac{\partial \Omega_{z_k}}{\partial A_{z_k}}\right)_{T_{z_k},V_{z_k},\mu_{z_k}}. \tag{A18}$$

By applying the perturbation formalism between the reference state (0) and the perturbed state (1), the surface tension is expressed as the ratio of the grand canonical function between the two states [cf. Eq. (A20)]. From the calculation of both the local configuration temperature and the total local chemical potential, we check that $T_{z_k}=T_{z_k'}=T$ and $\mu_{z_k}=\mu_{z_k'}$, respectively. Let us recall that the transformation carried out on the slab does not change its volume and allows us to write $d\mathbf{r}^N=d\mathbf{r}'^N$. These equalities lead to the expression given in Eq. (A22):

$$\gamma_{\mathrm{TA},z_k} = \left(\frac{\partial \Omega_{z_k}}{\partial A_{z_k}}\right)_{\mu_{z_k},V_{z_k},T_{z_k}} = \lim_{\epsilon\to 0} \frac{\Omega(Nz_k', Vz_k', Tz_k', A^{(1)}_{z_k'}) - \Omega(Nz_k, Vz_k, Tz_k, A^{(0)}z_k)}{\Delta A_\epsilon} \tag{A19}$$

$$= -\frac{k_B T}{\Delta A_\epsilon} \ln \frac{\Xi^{(1)}_{u_{z_k'} V_{z_k'} T_{z_k'}}}{\Xi^{(0)}_{u_{z_k} V_{z_k} T_{z_k}}} \tag{A20}$$

$$= -\frac{k_B T}{\Delta A_\epsilon} \ln \frac{\sum_{N_{z_k}}^{\infty} \exp\left(\frac{N_{z_k'}\mu_{z_k'}}{k_B T}\right) \int d\mathbf{r}'^N \exp\left(-\frac{\mathcal{U}^{(1)}_{z_k'}(\mathbf{r}'^N)}{k_B T}\right)}{\sum_{N_{z_k}}^{\infty} \exp\left(\frac{N_{z_k}\mu_{z_k}}{k_B T}\right) \int d\mathbf{r}^N \exp\left(-\frac{\mathcal{U}^{(0)}_{z_k}(\mathbf{r}^N)}{k_B T}\right)} \tag{A21}$$

$$= -\frac{k_B T}{\Delta A_\epsilon} \ln \frac{\int d\mathbf{r}^N \exp\left(-\frac{\mathcal{U}^{(1)}_{z_k'}(\mathbf{r}'^N)}{k_B T}\right)}{\int d\mathbf{r}^{N)} \exp\left(-\frac{\mathcal{U}z_k'^{(0)}(\mathbf{r}^N)}{k_B T}\right)} \tag{A22}$$

$$= -\frac{k_B T}{\Delta A_\epsilon} \times \ln \frac{\int d\mathbf{r}^N \exp\left(-\frac{(\mathcal{U}^{(1)}_{z_k'}(\mathbf{r}'^N) - \mathcal{U}^{(0)}_{z_k}(\mathbf{r}^N)}{k_B T}\right) \exp\left(-\frac{\mathcal{U}^{(0)}_{z_k}(\mathbf{r}^N)}{k_B T}\right)}{\int d\mathbf{r}^N \exp\left(-\frac{\mathcal{U}^{(0)}_{z_k}(\mathbf{r}^N)}{k_B T}\right)} \tag{A23}$$

$$= -\frac{k_B T}{2\Delta A_\epsilon} \ln \left\langle \exp\left(-\frac{\Delta \mathcal{U}_{z_k}}{k_B T}\right)\right\rangle_0. \tag{A24}$$

Equation (A24) gives the operational expression of the local surface tension calculated from the test-area method [8]. Within the assumption that the slabs can be treated independently, we numerically check that the total surface tension γ_{TA} is the sum of the local surface tension γ_{TA,z_k}.

APPENDIX B: LOCAL ENTROPY CALCULATION

The entropy variation ΔS can be calculated via the Widom insertion method using the expressions

$$\Delta S = S^{N+1} - S^N = -\frac{\partial \mu}{\partial T} \tag{B1}$$

$$= -\frac{\partial}{\partial T}[k_B T \ln \rho\Lambda^3 - k_B T \ln \langle \exp(-\Delta\mathcal{U}/k_B T)\rangle_{NVT}]$$

$$= -\left[k \ln \rho\Lambda^3 + kT\rho\Lambda^3 \frac{\partial}{\partial T}(\rho\Lambda^3) - k \ln \langle \exp(-\Delta\mathcal{U}/k_B T)\rangle_{NVT} - \frac{kT}{\langle \exp(-\Delta\mathcal{U}/k_B T)\rangle_{NVT}} \frac{\partial}{\partial T}(\langle \exp(-\Delta\mathcal{U}/k_B T)\rangle_{NVT})\right]. \quad \text{(B2)}$$

After further elaboration, the operational expression of the entropy variation is expressed as

$$\Delta S = -k_B \ln \rho\Lambda^3 + \frac{3k_B}{2} + k_B \ln \langle \exp(-\Delta\mathcal{U}/k_B T)\rangle_{NVT} + \frac{1}{T}\frac{\langle (\mathcal{U} + \Delta\mathcal{U})\exp(-\Delta\mathcal{U}/k_B T)\rangle_{NVT}}{\langle \exp(-\Delta\mathcal{U}/k_B T)\rangle_{NVT}} - \frac{1}{T}\langle \mathcal{U}\rangle_{NVT}, \quad \text{(B3)}$$

where U is the configurational energy of the system.

To calculate this difference of entropy between the two phases, we define a local total entropy variation $T\Delta S^*_{z_k}$ expressed as

$$\Delta S^*_{z_k} = -k_B \ln \rho_{z_k}\Lambda^3 + \frac{3k_B}{2} + k_B \ln \langle \exp(-\Delta\mathcal{U}_{z_k}/k_B T)\rangle_{NVT} + \frac{1}{T}\frac{\langle (\mathcal{U}_{z_k} + \Delta\mathcal{U}_{z_k})\exp(-\Delta\mathcal{U}_{z_k}/k_B T)\rangle_{NVT}}{\langle \exp(-\Delta\mathcal{U}_{z_k}/k_B T)\rangle_{NVT}} - \frac{1}{T}\langle \mathcal{U}_{z_k}\rangle_{NVT}. \quad \text{(B4)}$$

The first two first in Eq. (B4) correspond to the ideal term of the entropy property whereas the three other terms represent the excess contribution.

[1] A. Trokhymchuk and J. Alejandre, J. Chem. Phys. **111**, 8510 (1999).
[2] F. Goujon, P. Malfreyt, J. M. Simon, A. Boutin, B. Rousseau, and A. H. Fuchs, J. Chem. Phys. **121**, 12559 (2004).
[3] J. S. Rowlinson and B. Widom, *Molecular Theory of Capillarity* (Oxford, Clarendon Press, 1982).
[4] J. G. Kirkwood and F. P. Buff, J. Chem. Phys. **17**, 338 (1949).
[5] J. H. Irving and J. G. Kirkwood, J. Chem. Phys. **18**, 817 (1950).
[6] J. P. R. B. Walton, D. J. Tildesley, and J. S. Rowlinson, Mol. Phys. **48**, 1357 (1983).
[7] J. P. R. B. Walton, D. J. Tildesley, and J. S. Rowlinson, Mol. Phys. **58**, 1013 (1986).
[8] G. J. Gloor, G. Jackson, F. J. Blas, and E. Miguel, J. Chem. Phys. **123**, 134703 (2005).
[9] A. Z. Panagiotopoulos, Mol. Phys. **67**, 813 (1987).
[10] A. Z. Panagiotopoulos, N. Quirke, M. Stapleton, and D. J. Tildesley, Mol. Phys. **63**, 527 (1988).
[11] A. Z. Panagiotopoulos, Mol. Simul. **9**, 1 (1992).
[12] F. Goujon, P. Malfreyt, A. Boutin, and A. H. Fuchs, J. Chem. Phys. **116**, 8106 (2002).
[13] B. Widom, J. Stat. Phys. **19**, 563 (1978).
[14] C. A. Leng, J. S. Rowlinson, and S. Thompson, Proc. R. Soc. London, Ser. A **352**, 1 (1976).
[15] J. G. Powles, S. E. Baker, and W. A. B. Evans, J. Chem. Phys. **101**, 4098 (1994).
[16] J. G. Powles, B. Holtz, and W. A. B. Evans, J. Chem. Phys. **101**, 7804 (1994).
[17] F. Goujon, P. Malfreyt, and D. J. Tildesley, ChemPhysChem **5**, 457 (2004).
[18] F. Goujon, P. Malfreyt, and D. J. Tildesley, Mol. Phys. **103**, 2675 (2005).
[19] B. Widom, J. Chem. Phys. **39**, 2802 (1963).
[20] M. Guo and B. C. Y. Lu, J. Chem. Phys. **106**, 3688 (1997).
[21] M. C. Martin and J. I. Siepmann, J. Phys. Chem. B **102**, 2569 (1998).
[22] W. L. Jorgensen, J. D. Madura, and C. J. Swenson, J. Am. Chem. Soc. **106**, 6638 (1984).
[23] B. Smit, S. Karaborni, and J. L. Siepmann, J. Chem. Phys. **102**, 2126 (1995).
[24] N. Go and H. A. Scheraga, Macromolecules **9**, 535 (1976).
[25] P. Ungerer, A. Boutin, and A. H. Fuchs, Mol. Phys. **99**, 1423 (2001).
[26] H. H. Rugh, Phys. Rev. Lett. **78**, 772 (1997).
[27] O. G. Jepps, G. Ayton, and D. J. Evans, Phys. Rev. E **62**, 4757 (2000).
[28] G. Rickayzen and J. G. Powles, J. Chem. Phys. **114**, 4333 (2001).
[29] J. Delhommelle and D. J. Evans, J. Chem. Phys. **114**, 6229 (2001).
[30] A. Harasima, Adv. Chem. Phys. **1**, 203 (1958).
[31] B. D. Todd, D. J. Evans, and P. J. Daivis, Phys. Rev. E **52**, 1627 (1995).
[32] G. H. Peters and D. J. Tildesley, Phys. Rev. E **52**, 1882 (1995).
[33] J. A. Alejandre, D. J. Tildesley, and G. A. Chapela, Mol. Phys. **85**, 651 (1995).
[34] E. Diaz-Herrera, J. Alejandre, G. Ramirez-Santiago, and F. Forstmann, J. Chem. Phys. **110**, 8084 (1999).
[35] A. J. C. Ladd and L. V. Woodcok, Mol. Phys. **2**, 611 (1978).
[36] M. Mecke and J. Winkelmann, J. Chem. Phys. **107**, 9264 (1997).
[37] M. Mecke, J. Winkelmann, and J. Fischer, J. Chem. Phys. **110**, 1188 (1999).
[38] J. Janecek, J. Phys. Chem. B **110**, 6264 (2006).
[39] E. M. Blokhuis, D. Bedeaux, C. D. Holcomb, and J. A. Zollweg, Mol. Phys. **85**, 665 (1995).
[40] E. Salomons and M. Mareschal, J. Phys.: Condens. Matter **3**, 3645 (1991).
[41] R. W. Zwanzig, J. Chem. Phys. **22**, 1420 (1954).
[42] H. T. Davis and L. E. Scriven, Adv. Chem. Phys. **49**, 357 (1982).
[43] A. Ben-Naim and Y. Marcus, J. Chem. Phys. **81**, 2016 (1984).